



**HAL**  
open science

## Ca-Sr isotope and chemical evidence for distinct sources of carbonatite and silicate mantle metasomatism

Hongli Zhu, Dmitri Ionov, Long Du, Zhaofeng Zhang, Weidong Sun

### ► To cite this version:

Hongli Zhu, Dmitri Ionov, Long Du, Zhaofeng Zhang, Weidong Sun. Ca-Sr isotope and chemical evidence for distinct sources of carbonatite and silicate mantle metasomatism. *Geochimica et Cosmochimica Acta*, 2021, 312, pp.158-179. 10.1016/j.gca.2021.08.004 . hal-03402764

**HAL Id: hal-03402764**

**<https://hal.science/hal-03402764>**

Submitted on 16 Oct 2023

**HAL** is a multi-disciplinary open access archive for the deposit and dissemination of scientific research documents, whether they are published or not. The documents may come from teaching and research institutions in France or abroad, or from public or private research centers.

L'archive ouverte pluridisciplinaire **HAL**, est destinée au dépôt et à la diffusion de documents scientifiques de niveau recherche, publiés ou non, émanant des établissements d'enseignement et de recherche français ou étrangers, des laboratoires publics ou privés.



Distributed under a Creative Commons Attribution - NonCommercial 4.0 International License

# **Ca-Sr isotope and chemical evidence for distinct sources of carbonatite and silicate mantle metasomatism**

Hongli Zhu<sup>a,b,c</sup>, Dmitri A. Ionov<sup>\*d,e</sup>, Long Du<sup>f</sup>, Zhaofeng Zhang<sup>e,g</sup>, Weidong Sun<sup>a,b,c</sup>

<sup>a</sup> *Center of Deep Sea Research, Institute of Oceanography, Chinese Academy of Sciences, Qingdao 266071, China*

<sup>b</sup> *Laboratory for Marine Mineral Resources, Pilot National Laboratory for Marine Science and Technology (Qingdao), Qingdao 266237, China*

<sup>c</sup> *Center for Ocean Mega-Science, Chinese Academy of Sciences, Qingdao 266071, China*

<sup>d</sup> *Géosciences Montpellier, University of Montpellier, CNRS, Montpellier 34095, France*

<sup>e</sup> *State Key Laboratory of Isotope Geochemistry, Guangzhou Institute of Geochemistry, Chinese Academy of Sciences, Guangzhou 510640, China*

<sup>f</sup> *College of Earth Science and Engineering, Shandong University of Science and Technology, Qingdao 266590, China*

<sup>g</sup> *International Center for Planetary Science, College of Earth Sciences, Chengdu University of Technology, Chengdu 610059, China*

*8898 words in the main text, 4 tables, 9 figures, Supplementary material; 98 references*

1 **Abstract** (404 words)

2 Enrichments in light REE without concomitant enrichments in high-field-strength  
3 elements in mantle peridotites are usually attributed to inputs from carbonate-rich  
4 melts and referred to as ‘carbonatite’ metasomatism as opposed to interaction with  
5 evolved silicate melts. Alternatively, both enrichment types are ascribed to percolating  
6 volatile-bearing mafic liquids whose chemical signatures evolve from ‘silicate’ to  
7 ‘carbonatite’. Here we compare these models for peridotites in which these  
8 enrichment types are combined, as may be common in the mantle. We report new  
9 Ca-Sr-Nd isotope and chemical data for lherzolite and harzburgite xenoliths from  
10 Spitsbergen that were metasomatized, first, by silicate, then by carbonate-rich melts  
11 that formed carbonate-bearing pockets replacing earlier minerals. Seven crushed  
12 samples were treated with acetic acid that dissolved carbonates formed in the latest  
13 event, but not silicates. The leachates (acid-removed carbonates making up 0.6–1.4%  
14 of total sample mass) contain much more Sr than the residues after leaching  
15 (277–2923 vs. 16–60 ppm), have a greater overall  $^{87}\text{Sr}/^{86}\text{Sr}$  range (0.7049–0.7141 vs.  
16 0.7036–0.7055) and higher  $^{87}\text{Sr}/^{86}\text{Sr}$  in each sample than the residues. The leachates  
17 have lower  $\delta^{44/40}\text{Ca}$  range (0.17–0.68‰) than the residues (0.78–1.00‰), as well as  
18 lower  $\delta^{44/40}\text{Ca}$  than the residues in all samples but one. By and large, the carbonates  
19 are out of Ca-Sr isotope equilibrium with the host peridotites implying that the older  
20 silicate and younger carbonatite metasomatism were produced by different parental  
21 melts, thus supporting the existence of distinctive carbonate-rich metasomatic media  
22 in the lithospheric mantle, possibly including recycled materials.

23 The  $\delta^{44/40}\text{Ca}$  in the leachates (i.e. carbonates, 0.17–0.68‰) are well below bulk  
24 silicate Earth (BSE) estimates ( $0.94 \pm 0.05\%$ ) and  $\delta^{44/40}\text{Ca}$  in non-metasomatized  
25 melt-depleted mantle. Yet,  $\delta^{44/40}\text{Ca}$  in the non-leached whole rock (WR)  
26 carbonate-bearing samples (0.75–0.95‰) fall within, or are only slightly lower than,  
27 the BSE range. The  $^{87}\text{Sr}/^{86}\text{Sr}$  range in these WR samples (0.7030–0.7112) includes  
28 very high values for peridotites with large aggregates of dolomite and Mg-calcite. It

29 appears that both carbonatite and silicate metasomatism may produce  $\delta^{44/40}\text{Ca}$  values  
30 lower than the BSE such that Ca-isotope data cannot robustly tell apart these two  
31 enrichment types, yet carbonatite metasomatism may yield the lowest  $\delta^{44/40}\text{Ca}$ .  
32 Carbonates, even at small mass fractions, are significant hosts of Sr in the WR  
33 Spitsbergen peridotites (8–51 wt.% of Sr mass) because of very high Sr  
34 concentrations, but add little to WR Ca balance (3–12 wt.%). As a result, high Sr  
35 content and  $^{87}\text{Sr}/^{86}\text{Sr}$  ratios may be indices (though not definitive proofs) of  
36 carbonatite metasomatism in mantle rocks.

37

38 **Key words:** carbonatite metasomatism; silicate metasomatism; Ca isotopes; Sr  
39 isotopes; mantle xenolith; peridotite; Spitsbergen

## 1. INTRODUCTION

40

41

42 Studies of chemical and mineralogical composition of mantle rocks suggested that  
43 they were affected by two types of metasomatism, 'silicate' and 'carbonatite', the  
44 latter characterized by strong enrichments in light rare earth elements (LREE) at low  
45 high-field-strength elements (HFSE) (Ionov et al., 1993; Rudnick et al., 1993; Yaxley  
46 et al., 1991). These results implied an important, widespread role for carbonatite melts  
47 as agents of mantle metasomatism, despite the rarity of these melts at the Earth's  
48 surface (Hauri et al., 1993). However, other studies on mantle xenoliths and peridotite  
49 massifs inferred that enrichment patterns similar to those attributed to carbonate-rich  
50 melts could be produced by reactive percolation of volatile-bearing silicate melts.  
51 Numerical modeling of this process (Navon and Stolper, 1987) obtained a range of  
52 chemical patterns from a single parental liquid at different distances from its source as  
53 a result of chromatographic fractionation (due to different element compatibility),  
54 with 'carbonatite' signatures at the percolation front (e.g. Bodinier et al., 1990; Ionov  
55 et al., 2002a).

56 The existence of distinct, carbonatite and silicate, agents of mantle metasomatism  
57 can be ascertained using isotope compositions, which may differ in samples affected  
58 by media generated from different sources, but are similar in samples reworked by  
59 derivatives of a single initial agent. Here we present new Ca-Sr-Nd isotope and trace  
60 element data for a suite of mantle peridotites from the island of Spitsbergen that  
61 contain carbonate-bearing pockets of mantle origin replacing earlier minerals (Ionov  
62 et al., 1993; Ionov et al., 1996). Calcium and strontium are typical chemical  
63 components of carbonatites. The main objective of this study is to distinguish the  
64 Ca-Sr isotope inputs of the carbonates in the rocks using leaching with acetic acid that  
65 dissolves only carbonates. The data are used to evaluate directly the effects of  
66 carbonate-rich liquids on mantle metasomatism as well as to establish whether  
67 different types and stages of metasomatism were produced by distinct types and

68 sources of media.

69 Calcium is a major lithophile element in the Earth's mantle and crust (e.g.  
70 Hofmann, 1988). It has six naturally occurring stable isotopes ( $^{40}\text{Ca}$ ,  $^{42}\text{Ca}$ ,  $^{43}\text{Ca}$ ,  $^{44}\text{Ca}$ ,  
71  $^{46}\text{Ca}$  and  $^{48}\text{Ca}$ ) with ~10% mass difference ( $\Delta m/m$ ) between  $^{40}\text{Ca}$  and  $^{44}\text{Ca}$  (DePaolo,  
72 2004). Calcium isotopic compositions are usually expressed as delta notation, e.g.  
73  $\delta^{44/40}\text{Ca}$  relative to NIST SRM 915a:  $[(^{44}\text{Ca}/^{40}\text{Ca})_{\text{sample}}/(^{44}\text{Ca}/^{40}\text{Ca})_{\text{NIST-SRM-915a}} - 1] \times$   
74 1000.

75 The application of Ca stable isotopic composition in geosciences has rapidly  
76 developed in the last two decades because Ca isotopes show important fractionation at  
77 low temperatures near the Earth's surface, and are considered important indices of a  
78 wide range of biological and chemical processes in sedimentology, environmental  
79 geochemistry, weathering etc. (e.g. Blättler and Higgins, 2017; DePaolo, 2004; Fantle  
80 and Tipper, 2014; Farkaš et al., 2007; Skulan et al., 1997). Ca isotopes may also give  
81 new insights into global reservoirs and high-temperature processes in the Earth's  
82 interior and extraterrestrial samples (see Antonelli and Simon (2020) for a review).

83 Recent studies revealed significant Ca isotope variations in mantle-derived mafic  
84 igneous rocks (Huang et al., 2011; Liu et al., 2017a; Zhu et al., 2020; Zhu et al.,  
85 2018b) and carbonatites (Amsellem et al., 2020; Banerjee and Chakrabarti, 2019;  
86 Banerjee et al., 2021; Sun et al., 2021). Ca isotope variations were reported also for  
87 the lithospheric mantle and ascribed to additions of recycled crustal materials (Chen et  
88 al., 2018; Huang et al., 2011; Liu et al., 2017a; Zhu et al., 2020; Zhu et al., 2018b)  
89 and/or equilibrium and disequilibrium isotope fractionation at high temperatures  
90 during: (a) melt extraction (Chen et al., 2019; Kang et al., 2017), (b) reaction with  
91 silicate and carbonate-rich melts or fluids (Ionov et al., 2019; Kang et al., 2017; Kang  
92 et al., 2019; Kang et al., 2016; Zhao et al., 2017). This opens up new prospects in  
93 mantle studies, but also creates new challenges, in particular how to distinguish Ca  
94 isotope variations in mantle rocks produced by intra-mantle fractionation from those  
95 caused by mixing with recycled crustal materials.

96 An important notion in mantle studies is that of the Bulk Silicate Earth (BSE),  
97 sometimes called “primitive mantle” (PM), defined as silicate portion of the Earth as  
98 it existed after separation of the core but before it was differentiated to crust and  
99 heterogeneous mantle (Hofmann, 1997). Present-day mantle reservoirs were formed  
100 by melt extraction from the BSE (Workman and Hart, 2005), metasomatism and  
101 recycling of surface materials. The BSE composition may be evaluated using fertile  
102 mantle peridotites that experienced no melt extraction or metasomatism (Palme &  
103 O’Neill, 2003; McDonough & Sun, 1995). So far, the only robust  $\delta^{44/40}\text{Ca}$  estimate for  
104 the BSE ( $0.94 \pm 0.05\%$ , 2sd) has been given by Kang et al. (2017) based on 14  
105 xenoliths of non-metasomatized fertile lherzolites with  $\text{Al}_2\text{O}_3$  (3.7–4.7 wt.%) and CaO  
106 (3.2–4.0 wt.%) overlapping the PM estimates (~4.5 and 3.6%, respectively).

107 Kang et al. (2017) obtained a higher than BSE average  $\delta^{44/40}\text{Ca}$  ( $1.06 \pm 0.06\%$ , 2sd)  
108 for strongly melt-depleted (1.3–1.7 wt.%  $\text{Al}_2\text{O}_3$ ), non-metasomatized (LREE-depleted)  
109 peridotites and suggested that high degrees of melt extraction produce slightly higher  
110 (by ~0.12%)  $\delta^{44/40}\text{Ca}$  in residues. A similar  $\delta^{44/40}\text{Ca}$  range (and  $\delta^{44/40}\text{Ca}$  evolution  
111 trend during melting) was found by Chen et al. (2019) in melt-depleted lherzolites  
112 from Alpine massifs. Kang et al. (2017) also reported usually lower  $\delta^{44/40}\text{Ca}$  (0.25–  
113 0.96%) in metasomatized (LREE-enriched) peridotites, in particular for low-CaO ( $\leq 1$   
114 wt.%) rocks with Ca budget dominated by metasomatic inputs.

115 Strontium, like Ca, is an alkali earth element, but its BSE abundance is three orders  
116 of magnitude lower (20 vs. 25400  $\mu\text{g/g}$ ). Strontium is highly incompatible during  
117 peridotite melting because cation  $\text{Sr}^{2+}$  is much larger than  $\text{Ca}^{2+}$  such that Sr partition  
118 coefficients between clinopyroxene (major Sr host in common lherzolites) and mafic  
119 melts are well below unity (<https://earthref.org/KDD/e:38/>). Using the Rb-Sr  
120 radiogenic isotope system for dating mantle materials is problematic due to high  
121 mobility of these elements (e.g. Pearson et al., 2014), but the  $^{87}\text{Sr}/^{86}\text{Sr}$  ratios may  
122 indicate the sources of mantle-derived rocks and magmas (Hofmann, 2003), as well as  
123 recycling of crustal materials (e.g. Guo et al., 2020; Xu, 2002). The  $^{87}\text{Sr}/^{86}\text{Sr}$  ratios in

124 mantle rocks are affected both by their age and the evolution of the Rb/Sr ratio  
125 that may be hard to disentangle to identify sources of metasomatism. By comparison,  
126 Ca isotope compositions do not evolve with time, but may reveal mantle sources,  
127 mixing or, alternatively, mass-dependent fractionation during mantle processes.  
128 Overall, the evidence from Sr and Ca isotopes may be complementary.

129 Previous studies found carbonates usually associated with (Na,Al)-rich silicate  
130 glass in some Spitsbergen xenoliths (Ionov et al., 1993; Ionov et al., 1996). The  
131 carbonates do not represent quenched carbonatite liquids but are crystal cumulates  
132 from carbonate-rich silicate melts reacting with host peridotites (Ionov and Harmer,  
133 2002). Trace element patterns estimated for such liquids (Ionov, 1998) are consistent  
134 with many features of ‘carbonatite’ metasomatism (enrichments in LREE, Sr, Ba and  
135 negative HFSE anomalies). However, similar element patterns were found also in  
136 peridotites that contain no carbonates and attributed to reactive percolation and  
137 extreme fractionation of volatile-bearing silicate melts (Ionov et al., 2002a).

138 Overall, it remains uncertain whether the carbonates in mantle xenoliths from  
139 Spitsbergen and other worldwide localities (e.g. Dautria et al., 1992; Ionov et al.,  
140 2018; Laurora et al., 2001) originate from particular carbonate-rich liquids or are  
141 late-stage derivatives of evolving volatile-bearing silicate melts. In a more general  
142 sense, the ambiguity concerns the origin of chemical signatures usually seen as  
143 evidence for ‘carbonatite’ mantle metasomatism (e.g. Rivalenti et al., 2004; Tappe et  
144 al., 2017).

145 This uncertainty is addressed here using Ca-Sr isotope and chemical data on  
146 carbonate-bearing Spitsbergen xenoliths, notably by treating WR samples with acetic  
147 acid that dissolves only carbonates. Analyses of the leachates, residues and bulk-rocks  
148 discern metasomatic inputs of late-stage carbonates (extracted by leaching) from those  
149 of earlier events (hosted by residues). We show that trace element patterns and Ca-Sr  
150 isotope compositions of the leachates, hence carbonates, are distinct from those in the  
151 silicate minerals of the host peridotites. We infer that the carbonate pockets were

152 formed from specific carbonate-rich liquids responsible for ‘carbonatite’  
153 metasomatism. We further discuss the application of Ca-Sr isotope data to gain  
154 insights into the sources and mechanisms of metasomatism in the mantle.

155

## 156 **2. GEOLOGICAL SETTING AND SAMPLES**

157 Spitsbergen is the largest island of the Svalbard archipelago, the northwestern (NW)  
158 edge of the Eurasian continent. It was connected to Greenland until the opening of the  
159 North Atlantic Ocean, and is located now ~200 km east of the mid-ocean ridge (e.g.  
160 [Vagnes and Amundsen, 1993](#)), between the North Atlantic and the Arctic Oceans at  
161 similar distances from Norway, Greenland and the North Pole.

162 Mantle xenoliths reported here were collected in alkali basaltic rocks at three  
163 Quaternary eruption centers in NW Spitsbergen: Sverre, Halvdan and Sigurd (e.g.  
164 [Griffin et al., 2012](#)). Most of the xenoliths are coarse to medium-grained spinel  
165 lherzolites containing 5–12% clinopyroxene ([Ionov et al., 2002a](#); [Ionov et al., 1996](#));  
166 samples 26A and 318 are harzburgites ([Streckeisen, 1976](#)). The samples from Sverre  
167 are mainly ‘anhydrous’ lherzolites, while the Halvdan peridotites usually contain  
168 amphibole with modal abundances ranging from rare grains in sample 4-90-9 to 5–8%  
169 in samples 318 and 315-6. Samples 21-6 and 43-86 have accessory apatite ([S-Fig. 1a](#)  
170 in Electronic Appendix 2 (EA2)). The peridotites equilibrated at 840–990°C based on  
171 two-pyroxene thermometry ([Ionov et al., 2002a](#)). Sample 4A-90-1 from Sigurd is a  
172 coarse-grained clinopyroxene-amphibole vein.

173 The xenoliths contain carbonates as mosaic aggregates of dolomite and Mg-calcite  
174 with smooth curvilinear boundaries made up of interlocking grains 20–50 µm in size  
175 ([Ionov, 1998](#); [Ionov et al., 1993](#); [Ionov et al., 1996](#)). They mainly occur in irregularly  
176 distributed pockets that typically make up ≤ 2–3% of the rock and are 0.2–2 mm in  
177 size. The pockets also contain small (<100 µm) euhedral grains of clinopyroxene and  
178 olivine, Fe-Ni sulfides and (Na,Al)-rich silicate glass with micro-phenocrysts of  
179 Cr-rich spinel ([S-Fig. 1d-h, EA2](#)). The pockets replace minerals of host peridotite,

180 usually orthopyroxene, amphibole and spinel, that have embayed, resorbed outlines  
181 and spongy reaction zones. Less commonly the carbonates occur as mosaic aggregates  
182 in veins and at grain junctions of silicates (S-Fig. 1b-c, EA2).

183 Such assemblages closely resemble experimental and natural evidence for  
184 mantle-derived carbonatite metasomatism (e.g. Green and Wallace, 1988). Studies of  
185 melt and fluid inclusions in other carbonate-bearing, metasomatized mantle xenoliths  
186 suggest that carbonate segregations formed from initially homogeneous  
187 silicate-carbonate melts that separate into carbonatite and silicate components when  
188 they intrude and react with host peridotites (Frezzotti et al., 2002; Laurora et al.,  
189 2001).

190 The carbonate globules are larger and more abundant in four out of seven xenoliths  
191 selected for leaching (samples 43-86, 4-36-90, 4-90-9 and 21-6). Some carbonate  
192 aggregates are altered at rims to fine grained and turbid materials consisting of  
193 composite microcrystalline (usually magnesite-ankerite) spherules immersed in  
194 amorphous Mg-rich silicate material with low totals (S-Fig. 1g). They are common in  
195 samples SB-4 and 28B (Ionov et al., 1993), but their proportions relative to primary  
196 carbonates are negligible in large pockets (samples 43-86, 4-36-90, 4-90-9 and 21-6).

197 Textural evidence suggests that the Mg-Fe-rich carbonates formed by alteration of  
198 primary dolomite and Mg-calcite in contact with silicates during the eruption, likely  
199 due to heating and pressure drop. However, no evidence exists for the formation of  
200 additional carbonates in low-temperature processes. Na-rich silicate glass in contact  
201 with carbonates is not altered and contains fresh sulfide globules (Ionov et al., 1996).  
202 The silicate glass in the xenoliths is very different from the glass in the host basaltic  
203 rocks in terms of color, phenocryst assemblage and chemical composition, which  
204 rules out links with host magma infiltration (Ionov et al., 1993).

205 Previous chemical and isotope studies of Spitsbergen xenoliths, including those  
206 that contain no carbonates, found combined effects of three discrete evolution stages.  
207 (1) The protoliths for the lithospheric mantle were formed by melt extraction from

208 fertile mantle with melting degrees ranging from <10% for some lherzolites to 25%  
209 for the harzburgites in the Paleoproterozoic that depleted the rocks in incompatible  
210 elements (Choi et al., 2010; Ionov et al., 2002a). (2) The melting residues were then  
211 metasomatized by silicate liquids to form amphibole and apatite as well as enrich the  
212 residues in incompatible elements (Ionov et al., 2002a), radiogenic Sr isotopes  
213 (0.7025–0.7036) and non-radiogenic Nd isotopes (0.5123–0.5136) (Ionov et al.,  
214 2002b). (3) Ingress of carbonate-rich media formed discordant carbonate-bearing  
215 pockets shortly before the eruption of host magma (Ionov, 1998).

216 Ionov et al. (2002a) outlined two types of trace element patterns in WR samples  
217 and coarse silicate minerals of Spitsbergen xenoliths (Type-1 and Type-2) that  
218 combine features attributed to silicate or carbonatite metasomatism, e.g. negative  
219 Ti-Zr-Hf anomalies in Type-2 rocks and strongly fractionated LREE with high La/Ce  
220 (and H<sub>2</sub>O/Ce, Tang et al. (2020)) in Type-1 bulk-rocks and clinopyroxene. Ionov et al.  
221 (2002a) argued that the remarkable enrichments in the least compatible elements,  
222 along with fractionation of elements with similar compatibility, in Type 1 samples  
223 may not be due to mixing of melting residues with common enriched mafic melts but  
224 to extreme fractionation near melt percolation front. They used numerical modelling  
225 of reactive porous flow of volatile-bearing silicate liquids in depleted peridotites to  
226 explain their trace element patterns and Sr-Nd isotope ratios (Ionov et al., 2002a;  
227 Ionov et al., 2002b). Those studies, however, did not address specifically xenoliths  
228 containing late-stage carbonates and pockets of fine-grained minerals and silicate  
229 glass. They did not establish the provenance of carbonate-rich media responsible for  
230 carbonate formation, particularly whether they are related to late-stage derivatives of  
231 silicate metasomatism in the Spitsbergen mantle.

232

### 233 3. SAMPLE TREATMENT AND ANALYTICAL METHODS

234

235 The xenoliths analyzed in this study are listed in Table 1, along with a summary of

236 information on available data from this and previous studies.

### 237 **3.1 Leaching experiments**

238 Acid-leaching experiments were done on seven carbonate-bearing peridotites to  
239 obtain separately the compositions of carbonates and silicates (as well as spinel and  
240 apatite) in each sample. Our approach is different from that employed by [Ionov et al.](#)  
241 [\(1993\)](#) who leached two of these samples ([Table 1](#)) with 10% HNO<sub>3</sub> for about 20  
242 minutes in an ultrasonic bath, which did not only dissolve carbonates but may have  
243 also affected other phases, e.g. silicate glass. In this study, the samples were treated  
244 with dilute acetic acid (HAc), which dissolves carbonates while leaving silicate and  
245 oxide phases intact. Specifically, aliquots of 4–10 g of rock were crushed by hand to  
246 ≤1 mm in an agate mortar. These samples were transferred to centrifuge tubes and  
247 weighed. About 15 ml of 10% HAc were added to the centrifuge tubes, which usually  
248 produced gas bubbles; the tubes were shaken for about 30 min. The samples were  
249 centrifuged and the leachates (solutions with dissolved carbonates) extracted by  
250 pipette; the leaching residues were washed twice with MQ water, which was added to  
251 the initial leachates.

252 To convert the acetate salts in the leachates to nitrates and remove remaining HAc,  
253 the leachate solutions were dried and treated with concentrated HNO<sub>3</sub> several times  
254 on a hot plate at 150°C until clear solutions were obtained, then transferred to Teflon  
255 beakers. The solutions were dried, and dissolved in 2M HNO<sub>3</sub> for major and trace  
256 element and Sr-Nd-Ca isotopic analysis.

257 After the leachate extraction, the residues were dried overnight at 105°C and  
258 weighed to calculate the mass loss on leaching, and the relative mass of the carbonate  
259 and acid-resistant components in each sample. Finally, the leaching residues were  
260 ground to 200 mesh powder for analyses.

261

### 262 **3.2 Major and trace elements**

263 Major and trace element concentrations were obtained in this study for leachates

264 and residues from seven xenoliths, as well as for six WR samples (non-leached).  
265 Another six WR samples were analyzed for major elements only. We also use WR  
266 major and trace element data on 17 Spitsbergen xenoliths reported earlier (Ionov et al.,  
267 2002a; Ionov et al., 1993; Ionov et al., 1996).

268 The major and trace element analyses were done at the State Key Laboratory of  
269 Isotope Geochemistry (SKLIG), Guangzhou Institute of Geochemistry (GIG),  
270 Chinese Academy of Sciences (CAS). About 80 mg of residue or WR powder was  
271 fully digested in Teflon beakers with HF-HNO<sub>3</sub> mixtures placed in steel-jacketed  
272 PARR bombs following procedures reported in Wang et al. (2018). These solutions  
273 were used for both major and trace element, and Ca-Sr-Nd isotopic analyses.

274 Major elements (except Si) were analyzed by inductively coupled plasma atomic  
275 emission spectrometry (ICP-AES); Chinese reference samples GSR-1, GSR-2, GSR-3,  
276 SARM-4 and SY-4 were used for external calibration. Repeated analyses of USGS  
277 reference materials indicate external reproducibility better than 10%. Trace elements  
278 were determined by ICP mass spectrometry (ICP-MS) following procedures reported  
279 in Du et al. (2018) with reproducibility better than 5%.

280

### 281 3.3 Sr-Nd isotopes

282 Chemical separation and isotope analyses of Sr and Nd were done at the SKLIG-  
283 GIG-CAS. Aliquots of sample solution containing ~800 ng of Sr were transferred to a  
284 Teflon beaker, dried, and dissolved in 0.25 ml of 3 M HNO<sub>3</sub>. To separate Sr from  
285 sample matrix, the sample solution was loaded onto a column packed with 0.25 ml of  
286 Sr Spec resin (Zhu et al., 2018b). After elution by 6.5 ml of 3 M HNO<sub>3</sub>, Sr was  
287 collected in 3 ml of 0.05 M HNO<sub>3</sub>. Strontium isotopes were measured on a Nu Plasma  
288 1700 multi-collector (MC) ICP-MS instrument. The <sup>87</sup>Sr/<sup>86</sup>Sr ratios were corrected for  
289 instrumental mass fractionation by normalizing to <sup>88</sup>Sr/<sup>86</sup>Sr = 8.375209. The <sup>87</sup>Sr/<sup>86</sup>Sr  
290 values obtained for reference materials NBS-987 (0.710254 ± 0.000014; 2sd, n = 12)  
291 and BHVO-2 (0.703503 ± 0.000009; n = 1, internal precision) are consistent with

292 literature data (Table 2) (Charlier et al., 2006; Meng et al., 2019; Thirlwall, 1991;  
293 Weis et al., 2006).

294 More than half of the leachates, residues and WR samples are too low in Nd for  
295 precise Nd isotope analyses. Neodymium was purified using a two-column procedure  
296 reported in Du et al. (2019) and Ma et al. (2013). The first column filled with 1 g of  
297 AG50W-X12 (200–400 mesh) resin was eluted with 2.5 M HCl to extract the REE.  
298 Neodymium was separated from other REE on the second column filled with 1 g of  
299 Ln Spec (50–100 mesh) resin and eluted with 0.25 M HCl. The isotopic ratios were  
300 measured on a Nu Plasma 1700 MC-ICP-MS. The  $^{143}\text{Nd}/^{144}\text{Nd}$  values for reference  
301 materials JNdi ( $0.512111 \pm 0.000013$ ; 2sd,  $n = 13$ ) and W-2 ( $0.512512 \pm 0.000008$ ;  $n$   
302 = 1, internal precision) agree within error with literature data (Li et al., 2012; Luo et  
303 al., 2020; Tanaka et al., 2000) as shown in Table 2.

304

### 305 **3.4 Calcium isotopes**

306 Chemical purification and analyses of Ca isotope compositions were done at the  
307 SKLIG-GIG-CAS following procedures in Zhu et al. (2018a), Zhu et al. (2016) and  
308 Liu et al. (2017b). An aliquot of sample solution containing 30–50  $\mu\text{g}$  of Ca was  
309 mixed with a  $^{42}\text{Ca}$ - $^{43}\text{Ca}$  double-spike solution containing 8  $\mu\text{g}$  Ca, dried, re-dissolved  
310 in 0.1 ml of 1.6 M HCl, loaded onto a column filled with 1 ml of AG MP-50  
311 (100–200 mesh) and eluted with 1.6 M HCl. Most of the matrix was eluted with 17 ml  
312 of 1.6 M HCl, then Ca was collected in 27 ml of 1.6 M HCl. Samples low in CaO (< 3  
313 wt.%) were passed through the column twice. The Ca recovery was >99%. Column  
314 chemistry was run in batches of 20 samples; at least one reference material and blank  
315 were processed as unknowns with each batch. Total procedure blanks were 15–70 ng,  
316 which is negligible compared to 30–50  $\mu\text{g}$  of Ca loaded onto the column.

317 Calcium isotopic compositions were measured on a ‘Thermo Triton’ thermal  
318 ionization mass-spectrometer (TIMS). About 1  $\mu\text{l}$  10%  $\text{HNO}_3$  containing 5  $\mu\text{g}$  Ca was  
319 loaded onto the center of out-degassed single Ta (99.995%) filament. A droplet of 1  $\mu\text{l}$

320 activator (10% H<sub>3</sub>PO<sub>4</sub>) was loaded to cover the sample spot. A single sequence of cup  
321 configuration was adopted with <sup>40</sup>Ca, <sup>41</sup>K, <sup>42</sup>Ca, <sup>43</sup>Ca and <sup>44</sup>Ca collected in L2, C, H1,  
322 H2 and H3 Faraday cups, respectively. <sup>41</sup>K was measured to evaluate isobaric  
323 interference of <sup>40</sup>K on <sup>40</sup>Ca, and an online correction was done using <sup>40</sup>K/<sup>41</sup>K = 1.7384  
324 × 10<sup>-3</sup> Heuser et al. (2002). Instrumental fractionation was corrected using the  
325 <sup>42</sup>Ca-<sup>43</sup>Ca double spike method similar to that of Heuser et al. (2002) with the  
326 exponential fractionation law. The Ca isotope data are reported as δ<sup>44/40</sup>Ca relative to  
327 NIST SRM 915a. NIST SRM 915a and IAPSO seawater reference materials were  
328 routinely measured to monitor instrumental stability. Two standard deviation (2sd) of  
329 average δ<sup>44/40</sup>Ca for NIST SRM 915a analyzed in the course of this study was 0.12‰  
330 (n = 34). Three to seven aliquots of each sample solution were loaded on different  
331 filaments and measured separately; the reproducibility of δ<sup>44/40</sup>Ca in the duplicate  
332 analyses of each sample is ± 0.08‰ (2SE, see footnote of Table 3).

333 The δ<sup>44/40</sup>Ca values for NIST SRM 915a, IAPSO seawater and four USGS  
334 reference materials (DTS-1, DTS-2, PCC-1 and BHVO-2) measured in the same  
335 session, and literature data are listed in Table 2. Average δ<sup>44/40</sup>Ca values obtained for  
336 NIST SRM 915a and IAPSO seawater are -0.02 ± 0.12‰ (2sd, n = 21) and 1.82 ±  
337 0.10‰ (2sd, n = 10), respectively; those of DTS-1, DTS-2, PCC-1 and BHVO-2 are  
338 1.61 ± 0.09‰ (2sd, n = 3), 1.10 ± 0.11‰ (2sd, n = 3), 1.10 ± 0.08‰ (2sd, n = 3) and  
339 0.84 ± 0.09‰ (2sd, n = 5), respectively. These results are consistent with data  
340 reported in the literature (Amini et al., 2009; Farkaš et al., 2007; Feng et al., 2017; He  
341 et al., 2017; Huang et al., 2010; Valdes et al., 2014). Two WR samples were replicated  
342 by digestion of a separate powder batch; one leachate was duplicated by processing in  
343 column chemistry (Table 3). Duplicate δ<sup>44/40</sup>Ca values for all the three samples are  
344 within analytical uncertainty (Table 3).

345

346

#### 4. RESULTS

347

348 Major and trace element compositions of leachates, residues and WR xenoliths in  
349 this study are listed in [S-Tables 1 and 2](#) of Electronic Appendix 1 (EA1) along with  
350 relevant literature data ([Ionov et al., 2002a](#); [Ionov et al., 1993](#); [Ionov et al., 1996](#)). The  
351 Ca-Sr-Nd isotope compositions obtained in this study are given in [Tables 3 and 4](#).  
352 Acid leaching was used here to separate the metasomatic inputs of late-stage  
353 carbonates (extracted by leaching) from those of earlier melt extraction and silicate  
354 metasomatism hosted by residues ([Ionov et al., 2002a](#); [Ionov et al., 2002b](#)).

355

#### 356 **4.1 Chemical compositions**

357 The totals of the leachate analyses are low (46–63 wt.%) due to release of CO<sub>2</sub>  
358 from carbonates (44–48 wt.% in pure calcite and dolomite). The main components of  
359 the leachates are CaO, MgO and FeO. Their proportions range broadly and outline  
360 two end-members. Leachates from xenoliths 4-36-90, 4-90-9 and 21-6 contain 21–33  
361 wt.% CaO, 12–20% MgO and 2.2–3.4% FeO, with higher CaO than for MgO in each  
362 case. The leachate 43-86 has less CaO (20 wt.%) than MgO (27 wt.%). Leachates  
363 from the other three xenoliths (63-90-18, SB-4 and 28B) are low in CaO (9–15 wt.%)  
364 and have two to four times more MgO (34–37 wt.%) and 11–14 wt.% FeO.

365 Selected chemical data on WR samples and residues after leaching are plotted in  
366 [Fig. 1](#) vs. Al<sub>2</sub>O<sub>3</sub> together with data on fertile to melt-depleted peridotites from Tariat  
367 in Mongolia ([Ionov and Hofmann, 2007](#)). Leached residues of the Spitsbergen  
368 xenoliths generally have lower Sr, CaO and Ca/Al ratios than the WR samples, in line  
369 with the removal of Ca-Sr-rich carbonates. However, all but one residues have higher  
370 CaO and Ca/Al than melt-depleted mantle ([Fig. 1a](#)), but show no Sr enrichments ([Fig.](#)  
371 [1c](#)). The leachates contain much more Sr (277–2923 ppm) than the residues (16–60  
372 ppm) ([S-Table 2](#)). The Ca-rich leachates from three xenoliths have much more Sr  
373 (2337–2923 ppm) than the other four (277–455 ppm). Mass fractions of the leachates  
374 range from 0.6 to 1.4% of the bulk rocks ([Table 3](#)), in line with the mass fractions of  
375 carbonates (~1%) estimated by [Ionov et al. \(1993\)](#). Altogether, the data suggest that

376 leaching entirely removed the metasomatic carbonates from the WR samples.

377 [Ionov et al. \(2002a\)](#) outlined two types of PM-normalized ([McDonough and Sun,](#)  
378 [1995](#)) trace element patterns in WR Spitsbergen xenoliths. Our data ([Fig. 2](#)) show that  
379 the patterns for Type-1 peridotites are nearly flat for heavy to medium REE  
380 (HREE-MREE) with steep La-Ce-Pr inflections, while Type-2 peridotites show a  
381 continuous decrease in normalized REE from Ce to Ho ([Fig. 2a and c](#)). As a result,  
382 Type-1 peridotites have lower MREE/HREE and higher La/Ce ratios than Type-2  
383 peridotites.

384 Both types have strong negative Nb and Ta anomalies; all WR Type-1 peridotites  
385 and the majority of Type-2 peridotites show positive Sr anomalies ([Fig. 2b and d](#)).  
386 Because of the high MREE levels, Type-2 peridotites seem to have larger negative Zr,  
387 Hf and Ti anomalies ([Fig. 2d](#)) even though the abundances of these elements are  
388 similar to those in Type-1 peridotites. Three samples cannot be grouped with either  
389 Type-1 or Type-2 ([Fig. 2e, f](#)). Among the leached samples with mainly Ca-rich  
390 carbonates, one (4-36-90) is of Type 1 while the other three are of Type 2.

391 Trace element abundances and patterns for leaching residues and WR samples in  
392 this study ([Fig. 3](#)) are similar to those for two samples reported by [Ionov et al. \(1993\)](#).  
393 The concentrations of incompatible trace elements in the leachates in this study,  
394 calculated relative to the mass of leached materials, are lower than those reported by  
395 [Ionov et al. \(1993\)](#) when plotted relative to 1% of mass of WR samples. The leaching  
396 with 10% HNO<sub>3</sub> in the previous work may have dissolved more material than the  
397 leaching with 10% HAc in this study. The leachates contain more REE and large ion  
398 lithophile elements (Cs, Rb, Ba), but less HFSE than leaching residues and bulk rocks  
399 ([Figs. 3–5](#)). Besides, the leachates and the residues display the same Type-1 and  
400 Type-2 REE patterns, but the leachates have the deepest HFSE anomalies ([Fig. 5](#)).

401

## 402 **4.2 Sr-Nd isotope compositions**

403 The WR Spitsbergen xenoliths in this study show a broad overall <sup>87</sup>Sr/<sup>86</sup>Sr range

404 (0.7030–0.7112; Fig. 6a), with  $^{87}\text{Sr}/^{86}\text{Sr}$  values in four samples (0.708–0.711) much  
405 higher than in the other eleven samples (~0.703–0.704). Three out of seven leached  
406 samples have the most radiogenic Sr, the highest Sr (and Ca) concentrations in the  
407 leachates and also contain large, least altered carbonate pockets. In general, the WR  
408  $^{87}\text{Sr}/^{86}\text{Sr}$  ratios in this study are higher than those for pure clinopyroxene and  
409 amphibole separates from the same samples reported by Ionov et al. (2002b) (Fig. 7b  
410 and S-Fig. 2a). Our WR data show no apparent differences in  $^{87}\text{Sr}/^{86}\text{Sr}$  between  
411 Type-1 and Type-2 peridotites, unlike data of Ionov et al. (2002b) who found that  
412 clinopyroxene has less radiogenic  $^{87}\text{Sr}/^{86}\text{Sr}$  in Type-1 than in Type-2 peridotites. Few  
413 samples were measured for Nd isotopes here because of low Nd abundances. The WR  
414  $^{143}\text{Nd}/^{144}\text{Nd}$  range in this study (0.51218–0.51295; Fig. 6b) is narrower than for pure  
415 amphibole and clinopyroxene reported by Ionov et al. (2002b) (S-Fig. 2b).

416 The leachates, leaching residues and WR samples for each xenolith have distinct Sr  
417 isotopic compositions (Fig. 7b). The  $^{87}\text{Sr}/^{86}\text{Sr}$  in the leachates (0.7049–0.7141) have a  
418 wider range and are generally higher than in the residues (0.7036–0.7055). For a  
419 given xenolith, the WR sample has  $^{87}\text{Sr}/^{86}\text{Sr}$  ratios in-between those for leachates and  
420 residues.

421 Unlike for Sr isotope ratios, the leachates, residues and WR samples have similar  
422 Nd isotopic compositions (Fig. 7c), consistent with low Nd in the carbonates (Ionov,  
423 1998). The leachates contain only 1–7 wt.% of the total Nd in the bulk rocks (Table 3).  
424 The Sr and Nd isotope ratios in the leachates and the residues are positively correlated  
425 (Fig. 8b, c).

426

### 427 **4.3 Calcium isotopic compositions**

428 The  $\delta^{44/40}\text{Ca}$  values in the WR Spitsbergen peridotites range from 0.73 to 0.89‰  
429 (Fig. 6a), i.e. are slightly lower than the BSE estimate ( $0.94 \pm 0.05\%$ ; Kang et al.  
430 (2017)). There is no obvious difference between Type-1 and Type-2 xenoliths with  
431  $\delta^{44/40}\text{Ca}$  ranges of 0.78–0.89‰ and 0.73–0.87‰, respectively and between two

432 groups of leached samples based on Ca-Mg-Fe proportions in the leachates. The  
433  $\delta^{44/40}\text{Ca}$  range for leaching residues (0.78–1.00‰) extends to slightly higher values  
434 than for the WR samples, but the WR-residue differences do not exceed ~0.2‰ in  
435 individual xenoliths (Fig. 7a) and are principally within analytical uncertainty.

436 The leachates in six out of seven samples have significantly lower, and more  
437 variable,  $\delta^{44/40}\text{Ca}$  (0.17–0.68‰) than the WR samples and residues (Fig. 7a). The  
438 averages for the CaO-rich and Mg,Fe-rich leachates are very close (0.41‰ vs. 0.49‰).  
439 A single outlier is leachate from sample 43-86 that yielded anomalously high  $\delta^{44/40}\text{Ca}$ ,  
440  $1.47 \pm 0.03\text{‰}$  (2sd, n = 3) and  $1.46 \pm 0.08\text{‰}$  (2sd, n = 3) for two duplicates (Table 3),  
441 much higher than for the residue and WR sample. The Ca isotopic data for the  
442 leachate appear to be robust based on good reproducibility of the duplicated analyses,  
443 but the reasons for the anomalous values are not clear and are not further discussed  
444 below.

445 As shown in Table 3, the leached fractions account for only 3–12 wt.% Ca in each  
446 xenolith, such that the carbonates (with highly variable  $\delta^{44/40}\text{Ca}$  values) appear to have  
447 limited influence on  $\delta^{44/40}\text{Ca}$  of the WR samples. Like Sr and Nd isotope ratios, the  
448  $\delta^{44/40}\text{Ca}$  of the residues are negatively correlated with those of the leachates (Fig. 8a).

449

450

## 5. DISCUSSION

451

### 5.1 Major element composition and origin of leached carbonate materials

453 Electron probe analyses of carbonates in our samples (Ionov et al., 1996) show that  
454 the dolomite contains 28–40 wt.% CaO, 13–24 wt.% MgO and 0.3–5.0 wt.% FeO  
455 while the Mg-calcite contains 44–53 wt.% CaO, 3–11 wt.% MgO and 0.3–2.7 wt.%  
456 FeO. The leachates from three xenoliths that host large mosaic carbonate aggregates  
457 (4-36-90, 4-90-9 and 21-6) contain 21–33 wt.% CaO, 12–20% MgO and 2.2–3.4%  
458 FeO, with higher CaO than for MgO in each case. The leachates from these xenoliths  
459 appear to be derived essentially from the dolomite and Mg-calcite in such aggregates.

460 The leachate from sample 43-86 (that also has large pockets of mosaic Mg-calcite  
461 and dolomite) has less CaO (20 wt.%) than MgO (27 wt.%) and thus contains inputs  
462 from other carbonate materials. Leachates from the other three xenoliths (63-90-18,  
463 SB-4 and 28B) contain even less CaO (9–15 wt.%) and two to four times more MgO  
464 (34–37 wt.%) as well as 11–14 wt.% FeO. These ranges correspond to mixtures of  
465 dolomite and Mg-calcite with magnesite, ankerite  $[\text{Ca}(\text{Fe},\text{Mg})(\text{CO}_3)_2]$  and amorphous  
466 carbonate materials at margins of primary carbonate aggregates (Ionov et al., 1993).

467 Two formation modes could be envisaged for these materials. (1) Reaction of  
468 carbonate-rich melts with host peridotites at conditions (e.g. temperature increase  
469 related to basaltic magmatism) that do not allow precipitation of coarse Ca-rich  
470 carbonates. (2) Recrystallisation and alteration at margins of granular carbonate  
471 pockets. While they do not appear to be contaminated by host basalt or post-eruption  
472 alteration (that precipitates pure calcite), their composition may not be identical to  
473 that of granular metasomatic carbonates.

474

## 475 **5.2 ‘Carbonatite’ signatures and residence of Ca, Sr and Nd in WR peridotites**

476 Substantial differences between trace element patterns of leachates and bulk-rocks  
477 are seen in Figs. 3–5. The leachates show much greater enrichments of highly  
478 incompatible relative to moderately incompatible elements and negative HFSE  
479 anomalies, i.e. show essential features inferred for carbonatite metasomatism (e.g.  
480 Hauri et al., 1993; Rudnick et al., 1993) that are absent in the bulk-rocks. In particular,  
481 WR Type-1 peridotites and residues show no significant Ti-Zr-Hf anomalies and no  
482 fractionated Zr/Hf ratios while LREE/HREE ratios are much lower than in the  
483 leachates. These results reinforce the conjecture of Ionov et al. (2002a) that element  
484 patterns of Spitsbergen peridotites produced by percolation of volatile-bearing mafic  
485 melts are not as fractionated as in inferred media of carbonatite metasomatism.

486 In a more general sense this study suggests that enrichments by volatile-bearing  
487 silicate melts, on their own, are not likely to yield chemical signatures typical of

488 carbonatite metasomatism that require inputs from particular, carbonate-rich liquids.  
489 Further, the metasomatic effects of carbonate-rich liquids are less apparent in fertile  
490 lherzolites and previously enriched mantle than in highly melt-depleted protoliths  
491 (harzburgites, dunites) low in incompatible elements (e.g. Yaxley et al., 1998). The  
492 latter is the case for the Spitsbergen samples in which the patterns of bulk-rocks and  
493 leached residues are not very different in spite of the presence of carbonates.

494 The contribution of carbonates to the WR balance of Ca, Sr and Nd and their  
495 isotopic ratios in Spitsbergen xenoliths is evaluated here quantitatively from leaching  
496 data. Table 3 presents WR Ca-Sr-Nd isotopic compositions calculated from mass  
497 proportions of acid-leached material and residues in WR xenoliths, their Ca-Sr-Nd  
498 abundances, and  $\delta^{44/40}\text{Ca}$ ,  $^{87}\text{Sr}/^{86}\text{Sr}$  and  $^{143}\text{Nd}/^{144}\text{Nd}$  values (see also S-Tables 1-2 and  
499 Fig. 7). The measured WR compositions are similar to the estimates for the majority  
500 of the samples suggesting that the procedure is robust. The only outlier is sample  
501 4-36-90, with the calculated WR  $^{87}\text{Sr}/^{86}\text{Sr}$  value lower than the measured (Fig. 7b).  
502 This may be due to irregular carbonate distribution in the rocks, hence different  
503 carbonate mass fractions in the WR powder and sample duplicate used for leaching.

504 Significant differences in  $\delta^{44/40}\text{Ca}$  were found between the leachates (dissolved  
505 carbonates) and leaching residues (silicates), with  $\Delta^{44/40}\text{Ca}_{\text{leachate-residue}}$  from  $-0.83$  to  
506  $-0.17\text{‰}$  for six xenoliths, and  $0.69\text{‰}$  for anomalous sample 43-86 (Fig. 7a). By  
507 contrast, the WR  $\delta^{44/40}\text{Ca}$  values are within analytical uncertainty ( $\sim 0.1\text{‰}$ ) of those in  
508 the residues, indicating small effects of carbonates on  $\delta^{44/40}\text{Ca}$  of the WR xenoliths  
509 because of low Ca mass fractions hosted by the carbonates (3–12%; Table 3).

510 The relations between WR samples, leachates and residues are different for Sr and  
511 its isotope ratios. The leachates contain much more Sr than the residues (277–2923 vs.  
512 16–60 ppm; S-Table 2) and have higher  $^{87}\text{Sr}/^{86}\text{Sr}$  ratios in all the xenoliths. As a result,  
513  $^{87}\text{Sr}/^{86}\text{Sr}$  in the WR samples are significantly higher than in the residues, in particular  
514 for samples 4-36-90, 4-90-9 and 21-6 (cf. Fig. 7b). The leachates from these samples,  
515 with carbonates dominated by dolomite and Mg-calcite, have 2337–2923 ppm Sr

516 (35–51% of Sr mass in WR samples) with  $^{87}\text{Sr}/^{86}\text{Sr}$  ratios of 0.7136–0.7141.  
517 Therefore, in spite of the low mass fractions of the leached carbonates in the xenoliths  
518 (0.6–1.4%), they host a large share of Sr (8–51 wt.%) and greatly influence  $^{87}\text{Sr}/^{86}\text{Sr}$   
519 ratios in WR peridotites.

520 The limited Nd isotope data from leaching experiments show that  $^{143}\text{Nd}/^{144}\text{Nd}$  in  
521 leachates are close to, or slightly lower, than in residues and WR samples (Fig. 7c), in  
522 line with low Nd fractions hosted by carbonates (1–7 wt.%).

523 To sum up, the role of carbonates is very different in the WR balance of Ca, Sr and  
524 Nd abundances and isotopic compositions of Spitsbergen xenoliths. The metasomatic  
525 carbonates have very high Sr content and moderate to high  $^{87}\text{Sr}/^{86}\text{Sr}$  ratios, and thus  
526 may greatly affect the WR [Sr] and  $^{87}\text{Sr}/^{86}\text{Sr}$  values of mantle peridotites even at low  
527 mass fractions. These effects are the greatest for xenoliths with large, unaltered  
528 aggregates of dolomite and Mg-calcite.

529 These observations may help to trace metasomatic history also of some  
530 carbonate-free rocks. Carbonates are not stable in the uppermost mantle, and are  
531 transient phases rapidly consumed by reaction with orthopyroxene and spinel to form  
532 clinopyroxene and olivine (Brey et al., 1983; Dalton and Wood, 1995). This is why  
533 carbonates are very rare in mantle xenoliths. As the carbonates react out, Sr  
534 enrichments with high  $^{87}\text{Sr}/^{86}\text{Sr}$  ratios, initially residing in carbonates, may ultimately  
535 be hosted by clinopyroxene, amphibole, silicate glass, alkali feldspar, phosphates etc.;  
536 minerals replacing the carbonates may be zoned and/or include different generations  
537 (e.g. Aulbach et al., 2011; Coltorti et al., 1999; Deng et al., 2017; Guo et al., 2020;  
538 Ionov et al., 2006; Liu et al., 2012). As a result, unusually high Sr content and isotope  
539 ratios in carbonate-free peridotites and their minerals can be seen as indices of  
540 metasomatism by carbonate-rich melts that lost  $\text{CO}_2$  due to reaction with host mantle.  
541 Such reasoning was used by Hauri et al. (1993) to infer hotspot-related carbonatite  
542 metasomatism in the oceanic upper mantle based on clinopyroxene analyses. This  
543 study provides direct evidence for enrichment of the mantle in radiogenic Sr by

544 carbonate-rich media.

545

### 546 **5.3 Sr isotope evidence for distinct silicate and carbonatite metasomatic media**

547 The Sr isotope data on carbonates in the Spitsbergen xenoliths allow to elucidate  
548 the nature of their parental media. The  $^{87}\text{Sr}/^{86}\text{Sr}$  ratios of carbonate-bearing xenoliths,  
549 and in particular of leachates (i.e. carbonates) from these samples, are higher than  
550 those for leached residues as well as for silicate minerals separated from Spitsbergen  
551 xenoliths reported by [Ionov et al. \(2002b\)](#). The differences between the leachates and  
552 the silicates are the greatest for three xenoliths with large aggregates of dolomite and  
553 Mg-calcite ([Fig. 7b](#); [S-Fig. 2a](#)), i.e. the samples apparently most affected by putative  
554 carbonate-rich media and least affected by carbonate alteration during eruption. The  
555  $^{87}\text{Sr}/^{86}\text{Sr}$  range (0.7136–0.7141) in the leachates from these samples may be close to  
556  $^{87}\text{Sr}/^{86}\text{Sr}$  in these media. This unequivocally demonstrates the lack of Sr isotope  
557 equilibrium between the carbonates on the one hand, and coarse silicates in these  
558 xenoliths on the other hand. This further implies that the carbonates could not be  
559 formed from the liquids that metasomatized the silicate minerals because in such a  
560 case the carbonates and the silicates would have very similar  $^{87}\text{Sr}/^{86}\text{Sr}$  ratios. We see  
561 this is as a definitive proof that the carbonates were formed from a distinct  
562 carbonate-rich liquid unrelated to silicate metasomatism.

563 High  $^{87}\text{Sr}/^{86}\text{Sr}$  (~0.714) in metasomatic media require high long-term Rb/Sr ratios  
564 in their sources, e.g. due to high modal phlogopite or K-amphibole. High  $^{87}\text{Sr}/^{86}\text{Sr}$   
565 were reported for clinopyroxene and amphibole from MARID xenoliths (0.705–0.936  
566 [Fitzpayne et al., 2019](#); [Kramers et al., 1983](#)), carbonate mantle xenoliths (~0.709  
567 [Howarth et al., 2019](#)) and pyroxenites from North China (up to 0.715 [Dai et al., 2020](#)).  
568 Such domains may form in the mantle by fractionation of melts, e.g. at the top of a  
569 mantle plume, or more likely by incorporation of (a) blocks delaminated from the  
570 base of mantle lithosphere or (b) subducted crustal materials. For instance, [Hauri et al.](#)  
571 [\(1993\)](#) attributed high  $^{87}\text{Sr}/^{86}\text{Sr}$  (up to 0.713) in clinopyroxene in mantle xenoliths

572 from the Pacific to ‘carbonatite’ metasomatism by melts derived from recycled crustal  
573 components in the convecting mantle. Our data do not allow to distinguish mantle vs.  
574 crustal origins for the radiogenic Sr in the xenoliths in this study.

575 The very broad  $^{87}\text{Sr}/^{86}\text{Sr}$  range (0.7049–0.7141) of the leachates (i.e. carbonates),  
576 along with covariation of  $^{87}\text{Sr}/^{86}\text{Sr}$  in the leachates and the residues (Fig. 8b) indicate  
577 some limited isotope exchange between the carbonate-rich melt and host peridotites.  
578 The exchange may have continued during or after the formation of the carbonates, in  
579 particular for interstitial carbonate aggregates with greater surface relative to mass  
580 (S-Fig. 1b-c, EA2). This may be the reason why the carbonate-rich melts (and/or  
581 initially deposited dolomite and Mg-calcite in such pockets) reacted to form late-stage,  
582 Mg-Fe-rich carbonates common in many xenoliths in this study (S-Fig. 1G).

583 To sum up, we posit that granular dolomite and Mg-calcite formed from a parental  
584 carbonate-rich liquid that had  $^{87}\text{Sr}/^{86}\text{Sr}$  of  $\sim 0.714$ . The liquid, and possibly the initial  
585 carbonates, reacted with the host peridotites ( $^{87}\text{Sr}/^{86}\text{Sr} \sim 0.7025\text{--}0.7041$ ; Ionov et al.  
586 (2002b)) to form late-stage Mg-Fe carbonates. Sr-isotope exchange between the  
587 carbonate-rich melt and host rocks increased the  $^{87}\text{Sr}/^{86}\text{Sr}$  ratios in host peridotites, the  
588 more so in the samples with more carbonates, and produced the positive correlation of  
589  $^{87}\text{Sr}/^{86}\text{Sr}$  in leachates and residues, i.e. coexisting silicates and carbonates (Fig. 8b).

590 The  $^{87}\text{Sr}/^{86}\text{Sr}$  ratios in the residues of leaching that removed carbonates from the  
591 Spitsbergen xenoliths (0.7036–0.7055) are higher than in the depleted MORB mantle  
592 (DMM,  $\sim 0.7025$ ; Fig. 6a) (e.g. Carlson and Ionov, 2019; Stracke, 2012). This can be  
593 best explained by an earlier episode of ‘silicate’ metasomatism and possibly later  
594 exchanges with evolving carbonate-rich melts (see above).

595 Late-stage metasomatism taking place shortly before volcanic eruptions that bring  
596 mantle fragments to the surface has been documented in many xenolith suites.  
597 Remarkable examples of this phenomenon are xenoliths containing pockets and veins  
598 of silicate glass (e.g. Coltorti et al., 1999; Ionov et al., 1994), usually attributed to  
599 pre-eruption intrusion of carbonate-rich media, as well as sheared cratonic peridotites

600 with deformation accompanying melt metasomatism (e.g. [Agashev et al., 2013](#); [Ionov](#)  
601 [et al., 2017](#); [Katayama et al., 2009](#); [van der Meer et al., 2013](#)). Geophysical and  
602 experimental data (e.g. [Xu et al., 2020](#)) suggest that low-volume carbonate-rich melts  
603 can be pervasively present in the deep upper mantle. Such melts may trail upwelling  
604 mantle that generates xenolith-bearing magmas and react with their wall-rocks.

605

#### 606 **5.4 Ca isotope fractionation in the Spitsbergen mantle**

607 Radiogenic  $^{40}\text{Ca}$  enrichment from  $^{40}\text{K}$  decay can decrease  $\delta^{44/40}\text{Ca}$  values in rocks  
608 with old ages and high K/Ca ratios ([Fantle and Tipper, 2014](#)). The lithospheric mantle  
609 beneath Spitsbergen apparently formed in early Paleoproterozoic, most likely between  
610 1.7 and 2.7 Ga based on Lu-Hf and Re-Os isotope data ([Choi et al., 2010](#)). However,  
611 WR samples and residues in this study have low K/Ca ratios ( $<0.03$ ; [S-Table 1](#)) such  
612 that  $^{40}\text{K}$  decay could decrease  $\delta^{44/40}\text{Ca}$  of any of these samples only by  $<0.02\%$ , i.e.  
613 within analytical uncertainties, and thus could not affect the observed  $\delta^{44/40}\text{Ca}$  range.

614 As noted in Section 2, the  $\text{Al}_2\text{O}_3$  range in the Spitsbergen xenoliths indicates that  
615 their protoliths were residues of melt extraction ([Ionov et al., 2002a](#)) because  $\text{Al}_2\text{O}_3$  in  
616 mantle rocks is a robust melting index, little affected by metasomatism ([Pearson et al.,](#)  
617 [2014](#)). Peridotites formed by melt extraction from fertile mantle and unaffected by  
618 posterior metasomatism, like those from Tariat in Mongolia ([Carlson and Ionov, 2019](#);  
619 [Ionov and Hofmann, 2007](#)), define linear co-variation on CaO vs.  $\text{Al}_2\text{O}_3$  plots ([Fig.](#)  
620 [1a](#)), that overlaps the primitive mantle (PM) ([McDonough and Sun, 1995](#)). Some  
621 Spitsbergen peridotites plot close to this trend, but many have higher CaO and Ca/Al  
622 ratios at given  $\text{Al}_2\text{O}_3$  ([Fig. 1a, b](#)) indicating post-melting Ca enrichments. These  
623 enrichments are partly hosted by carbonates, but the fact that six out of seven leached  
624 residues show higher CaO and Ca/Al ratios than the melt-extraction trend ([Fig. 1a, b](#))  
625 suggest that metasomatic Ca additions may be mainly hosted by silicates. Overall, the  
626 Ca budget in the Spitsbergen xenoliths records the combined effects of melt extraction  
627 and enrichments by silicate and carbonatite media.

628

#### 629 5.4.1 $\delta^{44/40}\text{Ca}$ in products of melting and silicate metasomatism

630 Recent studies found that large degrees of partial melting may induce small, but  
631 conspicuous Ca isotopic fractionation, with higher  $\delta^{44/40}\text{Ca}$  in refractory melting  
632 residues than in coexisting melts. This inference is supported, first, by data on fertile  
633 to refractory mantle peridotites that show: (a) co-variation of  $\delta^{44/40}\text{Ca}$  with  $\text{Al}_2\text{O}_3$  and  
634 CaO (Fig. 9a-b); (b) higher (by  $\sim 0.1\text{‰}$ ) than in the BSE estimate  $\delta^{44/40}\text{Ca}$  values for  
635 melt-depleted (and non-metasomatized, i.e. LREE-depleted) low-Ca-Al lherzolites  
636 and harzburgites (e.g. Ionov et al., 2019; Kang et al., 2017). Furthermore, oceanic  
637 basalts show  $\delta^{44/40}\text{Ca}$  values that are consistently lower than in the BSE, e.g.  $0.83 \pm$   
638  $0.11\text{‰}$  (2sd,  $n = 21$ ) for MORB and  $0.80 \pm 0.08\text{‰}$  (2sd,  $n = 21$ ) for back-arc basin  
639 basalts (Chen et al., 2020; Zhu et al., 2020; Zhu et al., 2018b).

640 Chen et al. (2019) obtained average  $\delta^{44/40}\text{Ca}$  of  $0.94 \pm 0.11\text{‰}$  (2sd,  $n = 22$ ) for  
641 melt-depleted (2.0–3.4 wt.%  $\text{Al}_2\text{O}_3$ ) lherzolites from two tectonically emplaced  
642 massifs in the Alps. They failed to establish correlations of  $\delta^{44/40}\text{Ca}$  with  $\text{Al}_2\text{O}_3$  (i.e.  
643 melting degrees), apparently because of the lack of fertile lherzolites and complex  
644 melt impregnation in their samples. Furthermore, they reported  $\delta^{44/40}\text{Ca}$  below the  
645 BSE estimate both in residual harzburgites ( $0.89 \pm 0.09\text{‰}$ ; 2sd,  $n = 3$ ) and magmatic  
646 pyroxenites ( $0.86 \pm 0.10\text{‰}$ ; 2sd,  $n = 14$ ). We find confusing that Chen et al. (2019)  
647 used their data to define the  $\delta^{44/40}\text{Ca}$  range, alternately, for “Earth’s mantle”, “upper  
648 mantle” or “fertile mantle rocks” as  $0.94 \pm 0.10\text{‰}$  (2sd,  $n = 47$ ). The Earth’s mantle  
649 is heterogeneous, with  $\delta^{44/40}\text{Ca}$  well beyond the above range reported both for  
650 xenoliths of the lithospheric mantle (e.g. Chen et al., 2018; Ionov et al., 2019; Kang et  
651 al., 2019; Kang et al., 2020) and asthenosphere-derived magmatic rocks (see above).  
652 Further, the above range cannot refer to “fertile mantle” because Chen et al. (2019)  
653 reported data on melt-depleted peridotites overprinted by melt infiltration (without  
654 trace element data to evaluate possible metasomatic inputs).

655 The  $\text{Al}_2\text{O}_3$  content in leached residues in this study is much lower than in the BSE

656 (1.30–2.45 vs. 4.45 wt.%; [McDonough and Sun \(1995\)](#)) indicating that they  
657 experienced ~10–25% of partial melting ([Herzberg, 2004](#)). The  $\delta^{44/40}\text{Ca}$  values of  
658 melting residues with this  $\text{Al}_2\text{O}_3$  range should be ~0.12–0.04‰ higher than in the  
659 BSE based on equilibrium fractionation modeling (Fig. 9a-b [Chen et al., 2019](#); [Kang](#)  
660 [et al., 2017](#)). By contrast, the  $\delta^{44/40}\text{Ca}$  values for six out of seven leached samples  
661 (0.78–0.90‰, av.  $0.83 \pm 0.09\%$ , 2sd) and 16 out of 17 WR Spitsbergen samples  
662 (0.73–0.89‰, av.  $0.83 \pm 0.10\%$ , 2sd) are lower than the BSE estimate ( $0.94 \pm 0.05\%$ ;  
663 [Kang et al. \(2017\)](#)) and for non-metasomatized (from trace element data) fertile and  
664 melt-depleted peridotites in the literature ([Fig. 9](#)). The  $\delta^{44/40}\text{Ca}$  values in the majority  
665 of the Spitsbergen samples are below the BSE range also if the uncertainty of  
666 individual analyses is considered ([Fig. 9](#)). We conclude that the silicate metasomatism  
667 decreased  $\delta^{44/40}\text{Ca}$  values in the Spitsbergen lithospheric mantle by 0.1–0.2‰ relative  
668 to the likely range of ~1.0–1.1‰ in the initial melting residues (e.g. [Kang et al.,](#)  
669 [2017](#)).

670 Earlier xenolith studies inferred that metasomatism by silicate melts may decrease  
671  $\delta^{44/40}\text{Ca}$  in fertile or melt-depleted peridotites (e.g. [Kang et al., 2017](#)), but its effects  
672 on Ca isotopes continue to be debated. [Kang et al. \(2019\)](#) reported low  $\delta^{44/40}\text{Ca}$  values  
673 (0.65–0.87‰), correlated with  $(\text{Gd}/\text{Yb})_{\text{N}}$ , for Ca-Fe-rich lherzolites and wehrlites  
674 from Tok in the SE Siberian craton formed by reaction of lherzolites and harzburgites  
675 with silica-undersaturated partial melts. [Kang et al. \(2019\)](#) used equilibrium isotope  
676 fractionation modeling to infer that the Tok mantle was metasomatized by low-  
677  $\delta^{44/40}\text{Ca}$  liquids generated from eclogites. The  $\delta^{44/40}\text{Ca}$  values of leached Spitsbergen  
678 xenoliths are not correlated with  $(\text{Gd}/\text{Yb})_{\text{N}}$ , which argues against metasomatism by  
679 silicate melts from eclogite-rich sources. We see no reason to link these values to  
680 kinetic fractionation (e.g. [Zhao et al., 2017](#)) either because our samples show no  
681 modal or chemical (e.g. Fe enrichments) heterogeneities indicative of such a process.

682 Overall, the  $\delta^{44/40}\text{Ca}$  range in the leaching residues, hence in the Spitsbergen mantle  
683 before the most recent enrichment event, can be explained by a combination of melt

684 extraction, that moderately increased  $\delta^{44/40}\text{Ca}$  values, and subsequent silicate-melt  
685 metasomatism that brought  $\delta^{44/40}\text{Ca}$  in the melting residues below the BSE range.

686

#### 687 *5.4.2 Carbonatite Metasomatism*

688 The effects of carbonatite metasomatism on  $\delta^{44/40}\text{Ca}$  of mantle peridotites can be  
689 directly evaluated using data on carbonate-bearing xenoliths. [Ionov et al. \(2019\)](#)  
690 reported leaching data on xenoliths from the Obnazhennaya (Obn) kimberlite on the  
691 NE Siberian craton that contain carbonates texturally equilibrated with silicates. The  
692  $\delta^{44/40}\text{Ca}$  values in leachates from these samples (0.82–0.84‰) are similar to those for  
693 leached residues (0.70–0.84‰) within analytical uncertainty, which [Ionov et al. \(2019\)](#)  
694 attributed to Ca isotope equilibration of the carbonates with silicates ([Fig. 8a](#)).

695 By contrast, the carbonates in the Spitsbergen xenoliths mainly occur in texturally  
696 discordant pockets and veins, and differ strongly in Ca and Sr isotopic compositions  
697 from the leached silicate residues ([Fig. 7](#)). These carbonates are usually enclosed in  
698 Na,Al-rich silicate glass and fine-grained aggregates of silicates and spinel formed by  
699 reaction of carbonate-rich melts with host mantle ([Ionov, 1998; Ionov et al., 1996](#)), i.e.  
700 are out of chemical equilibrium with coarse silicates and have little direct contact with  
701 them. This, together with the short duration of the melt-rock reaction, may explain  
702 why the parental carbonate-rich melts did not attain Ca-Sr isotope equilibrium with  
703 the host mantle. The broad ranges of  $\delta^{44/40}\text{Ca}$  (0.17–0.68‰) and  $^{87}\text{Sr}/^{86}\text{Sr}$   
704 (0.7049–0.7141) in the leachates may be related to different amounts of the  
705 carbonate-rich melts and extents of isotopic exchange with host peridotites.

706 The differences between  $\delta^{44/40}\text{Ca}$  values of bulk (0.73–0.95‰) and leached  
707 (0.78–1.00‰) Spitsbergen xenoliths ([Figs. 6a and 7a](#)) are minor and imply limited  
708 bulk contributions from carbonatite metasomatism. This observation is consistent with  
709 Ca-isotope data on relevant mantle rocks from the literature. The  $\delta^{44/40}\text{Ca}$  values in the  
710 majority of carbonate-bearing Obn xenoliths are only 0.10–0.15‰ lower than the  
711 BSE estimate ([Fig. 9; Ionov et al. \(2019\)](#)). Few mantle xenoliths presumably affected

712 by carbonatite metasomatism reported in [Ionov et al. \(2019\)](#) and [Kang et al. \(2017\)](#)  
713 deviate by  $>0.3\%$  from the BSE estimate. The greatest metasomatism-induced Ca  
714 isotope effects are found in rocks with low pre-metasomatic Ca content that had high  
715 Ca additions and developed high Ca/Al ratios. Mass balance estimates show that the  
716 carbonates only account for 3–12% of Ca in the WR Spitsbergen xenoliths ([Table 3](#)),  
717 in line with the relatively low Ca/Al ratios ( $<2$ ) in these xenoliths ([Fig. 9c](#)).

718 To sum up, both carbonatite and silicate metasomatism reduced  $\delta^{44/40}\text{Ca}$  values of  
719 Spitsbergen peridotites and thus contributed to Ca isotope mantle heterogeneity. Both  
720 processes may result in lower  $\delta^{44/40}\text{Ca}$  values in mantle peridotites than in the BSE or  
721 melting residues such that Ca isotopes cannot robustly distinguish between these two  
722 types of mantle metasomatism ([Ionov et al., 2019](#)). On the other hand, the very low  
723  $\delta^{44/40}\text{Ca}$  in acid-leached materials from some carbonate-bearing Spitsbergen xenoliths,  
724 together with literature data on refractory peridotites with high Ca/Al, indicate that  
725 carbonatite metasomatism has a potential to yield the lowest  $\delta^{44/40}\text{Ca}$  in the mantle.

726

## 727 **5.5 Sources of carbonatites and carbonate-rich media of mantle metasomatism**

728 The isotopic signatures of metasomatism in the lithospheric mantle are related to  
729 the nature and sources of its media. An important issue is the share of carbonates in  
730 such media. Early experimental data and studies of mantle xenoliths evoked sodic  
731 dolomitic carbonate melts (e.g. [Yaxley et al., 1991](#)) while studies of  $\text{CO}_2$ -rich magmas  
732 (carbonatites and kimberlites) suggest that near-solidus melts of carbonated peridotite  
733 must be silicate-dominated with only dilute carbonate contents (e.g. [Tappe et al.,](#)  
734 [2017](#)). Furthermore, discrete  $\text{CO}_2$ -rich magma batches with different  $\delta^{44/40}\text{Ca}$  ratios  
735 may be derived from mixed sources in the convecting upper mantle ([Tappe et al.,](#)  
736 [2020](#)). The common association of carbonates in the Spitsbergen xenoliths with  
737 silicate glass and fine-grained silicates suggest that their parental liquids contain  
738 silicate components, but their share cannot be constrained from our data.

739 Carbonate-rich liquids generated both from ‘juvenile’ carbonated mantle and

740 sources containing subducted carbonates were recently evoked to explain the origin of  
741 carbonatites and kimberlites (e.g. [Banerjee and Chakrabarti, 2019](#); [Tappe et al., 2017](#)).  
742 [Ionov et al. \(2019\)](#) argued that recycling of carbonates, that show a broad  $\delta^{44/40}\text{Ca}$   
743 range, may not always alter the Ca isotopic composition in global mantle. [Banerjee](#)  
744 [and Chakrabarti \(2019\)](#) reported a  $\delta^{44/40}\text{Ca}$  range of 0.6–1.1‰, that overlaps the BSE  
745 estimate, for seven carbonatites from India and explained it by mixing of the plume  
746 end-member with recycled carbonates. [Amsellem et al. \(2020\)](#) obtained a much lower  
747 average  $\delta^{44/40}\text{Ca} = 0.26 \pm 0.25\text{‰}$  (2 sd, n = 50) for Ca-Mg-Fe carbonatites and argued  
748 that it reflects the incorporation of isotopically light marine carbonates into their  
749 mantle sources. By contrast, [Sun et al. \(2021\)](#) reported primary carbonatite and  
750 associated silicate rocks that are rather homogeneous in Ca isotope compositions that  
751 are comparable to those of basalts, which implies that the carbonatites are generated  
752 from a ‘juvenile’ mantle source without requiring the involvement of recycled  
753 carbonates. [Banerjee et al. \(2021\)](#) found BSE-like  $\delta^{44/40}\text{Ca}$  values in carbonatites older  
754 than 0.3 Ga, but low  $\delta^{44/40}\text{Ca}$  values (0.63‰, n=29) in younger carbonatites. While the  
755 topic may require further investigation, it is evident that carbonate-rich mantle melts  
756 may have both BSE-like and low  $\delta^{44/40}\text{Ca}$  values. This is consistent with inferences in  
757 this study that Ca isotope data cannot robustly distinguish carbonate and silicate  
758 mantle metasomatism (see the previous section).

759 This study found lower  $\delta^{44/40}\text{Ca}$  than for the BSE in the carbonates of mantle origin  
760 in Spitsbergen xenoliths. It appears that carbonatite metasomatism generally lowers  
761  $\delta^{44/40}\text{Ca}$  in mantle rocks, likely including basalt source regions ([Huang et al., 2011](#);  
762 [Ionov et al., 2019](#); [Kang et al., 2017](#); [Kang et al., 2016](#); [Liu et al., 2017a](#)). However,  
763 the limited available data also suggest that carbonatite metasomatism may not change  
764  $\delta^{44/40}\text{Ca}$  in the lithospheric mantle very much, except for rare highly refractory  
765 peridotites ([Ionov et al., 2019](#)), the latter are insignificant in mantle magma sources.

766

767

## 6. SUMMARY OF CONCLUSIONS

768

769 Leaching of peridotite xenoliths from Spitsbergen with acetic acid extracted  
770 carbonates formed in the latest metasomatic event and thus allowed to distinguish  
771 chemical and Ca-Sr-isotope imprints of their parental carbonate-rich melts from the  
772 combined effects of melt extraction and silicate metasomatism in leaching residues.

773 PM-normalized trace element patterns of the leached carbonates, unlike silicate  
774 residues, show distinctive indices (LREE-enrichments, HFSE-depletions) of  
775 carbonatite mantle metasomatism, suggesting that it necessitates specific  
776 carbonate-rich liquids rather than fractionation products of volatile-bearing silicate  
777 melts.

778 The carbonates are out of Ca-Sr isotope equilibrium with the silicates in the  
779 Spitsbergen peridotites implying that the silicate and carbonatite metasomatism are  
780 produced by different parental melts from distinct sources. This proves the existence  
781 of distinctive carbonate-rich metasomatic media in the lithospheric mantle.

782 The Spitsbergen carbonates are rich in Sr (277–2923 ppm) and have high  $^{87}\text{Sr}/^{86}\text{Sr}$   
783 (0.7049–0.7141). These signatures are retained in host peridotites when the transient  
784 carbonates react out to form Ca-rich silicates. High [Sr] and  $^{87}\text{Sr}/^{86}\text{Sr}$  may be indices  
785 (though not definitive proofs) of carbonatite metasomatism in mantle rocks.

786 The ranges of  $^{87}\text{Sr}/^{86}\text{Sr}$  (0.7136–0.7141) and  $\delta^{44/40}\text{Ca}$  (0.35–0.45‰) in leachates  
787 from three peridotites with large aggregates of dolomite and Mg-calcite constrain  
788 their values in sources of putative carbonate-rich media that either had high long-term  
789 Rb/Sr ratios or included recycled materials.

790 Both carbonatite and silicate metasomatism may produce  $\delta^{44/40}\text{Ca}$  values lower than  
791 the BSE, such that that Ca-isotope data cannot robustly tell apart these two  
792 enrichment types, yet carbonatite metasomatism may yield the lowest  $\delta^{44/40}\text{Ca}$ .

793

794

#### ACKNOWLEDGEMENTS

795 We are grateful to Yajun An, Fang Liu, Jinting Kang, Jianghao Bai, Wei Wu and Zebin Luo  
796 for help with analyses and discussions. This study was supported by grants from the National

797 Natural Science Foundation of China (No. 41773009 and 41873002) and the Programme  
798 National de Planétologie (PNP) of CNRS/INSU/CNES (grants to DAI in 2018-2019). DAI  
799 acknowledges Chinese Academy of Sciences President's International Fellowship Initiative  
800 (PIFI) for Visiting Scientists in 2019 (Grant No. 2017VCA0009). We appreciate constructive  
801 comments of S. Aulbach, S. Tappe, two anonymous reviewers and AE (A. Stracke).

802

## 803 **Figure Captions**

804 **Fig. 1.** Co-variation plots for (a) CaO (wt.%), (b) Ca/Al ratios and (c) Sr (ppm)  
805 versus Al<sub>2</sub>O<sub>3</sub> (wt.%) in whole rock (WR) peridotite xenoliths from Spitsbergen (Spi)  
806 (Ionov et al., 2002a) and in acid-leached samples of the same xenoliths (this study).  
807 Also shown are the primitive mantle (PM, [McDonough and Sun, 1995](#)) and WR  
808 peridotite xenoliths from Tariat (Tar) in Mongolia ([Ionov, 2007](#); [Ionov and Hofmann,](#)  
809 [2007](#)) that define a regular melt extraction trend (grey area in (a)), experienced no or  
810 little metasomatism after melting, and are similar in composition to depleted MORB  
811 mantle ([Carlson and Ionov, 2019](#)). Some Spitsbergen peridotites plot above the fields  
812 of the Tariat xenoliths due to metasomatic enrichments in Ca and Sr. Both leached and  
813 non-leached Spitsbergen xenoliths are enriched in Ca suggesting that much Ca resides  
814 in silicates. By contrast, non-leached bulk-rocks contain more Sr than acid-leached  
815 xenoliths because the carbonates may host more Sr than silicates.

816 **Fig. 2.** Primitive mantle-normalized ([McDonough and Sun, 1995](#)) REE (left  
817 column) and multi-element abundance patterns for whole-rock Spitsbergen peridotites.  
818 Data and rock types are after [Ionov et al. \(2002a\)](#).

819 **Fig. 3.** Comparison of trace element concentrations of leachates (Leach), leached  
820 residues (Res) and whole rocks (WR) for samples SB-4 and 43-86 in this study with  
821 leaching data of the same samples from [Ionov et al. \(1993\)](#) assuming that leached  
822 materials make up 1 wt.% of bulk rocks. The inferred element concentrations in the  
823 leached materials after [Ionov et al. \(1993\)](#) are much higher because they employed  
824 diluted HNO<sub>3</sub>, which dissolved not only carbonates as in this study, but also extracted  
825 trace elements from silicates.

826 **Fig. 4.** Primitive mantle-normalized ([McDonough and Sun, 1995](#)) REE patterns

827 for leachates (Leach) , residues (Res) and whole-rocks (WR) of carbonate-bearing  
828 peridotites.

829 **Fig. 5.** PM-normalized (McDonough and Sun, 1995) multi-element abundance  
830 patterns for leachates, residues and whole-rocks of carbonate-bearing peridotites.

831 **Fig. 6.** Plots of  $\delta^{44/40}\text{Ca}$  vs. (a)  $^{87}\text{Sr}/^{86}\text{Sr}$  and (b)  $^{143}\text{Nd}/^{144}\text{Nd}$  for leachates (Leach),  
832 residues (Res) and whole-rocks (WR) of Spitsbergen xenoliths. The blue horizontal  
833 line and grey bar represent the  $\delta^{44/40}\text{Ca}$  estimate for the BSE (Kang et al., 2017). The  
834 vertical dashed lines represent  $^{87}\text{Sr}/^{86}\text{Sr}$  and  $^{143}\text{Nd}/^{144}\text{Nd}$  for three types of the depleted  
835 MORB mantle (DMM): D-DMM, DMM and E-DMM after Workman and Hart  
836 (2005).

837 **Fig. 7.** Comparisons of (a)  $\delta^{44/40}\text{Ca}$ , (b)  $^{87}\text{Sr}/^{86}\text{Sr}$  and (c)  $^{143}\text{Nd}/^{144}\text{Nd}$  in leachates  
838 (Leach), residues (Res) and whole-rocks (WR) for seven carbonate-bearing  
839 Spitsbergen xenoliths as well as Sr and Nd isotopic ratios of cpx (Ionov et al., 2002b).

840 **Fig. 8.** Co-variation plots of  $\delta^{44/40}\text{Ca}$  (a),  $^{87}\text{Sr}/^{86}\text{Sr}$  (b) and  $^{143}\text{Nd}/^{144}\text{Nd}$  (c) for  
841 leachates and leaching residues in individual xenoliths. from Spitsbergen (Spi). Also  
842 shown are leachates and leaching residues in metasomatized, carbonate-bearing  
843 Obnazhennaya (Obn) peridotites (Ionov et al., 2019). Thick grey lines represent equal  
844 Ca-Sr-Nd isotopic values in leachates and leaching residues.

845 **Fig. 9.** Co-variation plots of  $\delta^{44/40}\text{Ca}$  versus wt.%  $\text{Al}_2\text{O}_3$  (a), wt.% CaO (b) and  
846 Ca/Al (c) in WR xenoliths and leaching residues (Res) of Spitsbergen (Spi) xenoliths.  
847 Also shown are melt-depleted peridotites from Tariat (Mongolia), and metasomatized,  
848 carbonate-bearing Obnazhennaya peridotites (Ionov et al., 2019; Kang et al., 2017).  
849 The blue horizontal line and gray bar represent estimated  $\delta^{44/40}\text{Ca}$  of the BSE and 2sd  
850 of the BSE estimate (Kang et al., 2017). The  $\delta^{44/40}\text{Ca}$  in the melt-depleted peridotites  
851 from Tariat and Obnazhennaya are negatively correlated with  $\text{Al}_2\text{O}_3$  and CaO. The  
852 leached Spitsbergen xenoliths display a negative  $\delta^{44/40}\text{Ca}$  vs.  $\text{Al}_2\text{O}_3$  correlation, but  
853 their  $\delta^{44/40}\text{Ca}$  values are lower than those for non-metasomatized melting residues  
854 from the literature.

855

856

## REFERENCES

857

858 Agashev A. M., Ionov D. A., Pokhilenko N. P., Golovin A. V., Cherepanova Y. and Sharygin I.  
859 S. (2013) Metasomatism in lithospheric mantle roots: Constraints from whole-rock and  
860 mineral chemical composition of deformed peridotite xenoliths from kimberlite pipe  
861 Udachnaya. *Lithos* **160–161**, 201-215.

862 Amini M., Eisenhauer A., Böhm F., Holmden C., Kreissig K., Hauff F. and Jochum Klaus P.  
863 (2009) Calcium Isotopes ( $\delta^{44}\text{Ca}$ ) in MPI - DING Reference Glasses, USGS Rock  
864 Powders and Various Rocks: Evidence for Ca Isotope Fractionation in Terrestrial Silicates.  
865 *Geostand. Geoanal. Res.* **33**, 231-247.

866 Amsellem E., Moynier F., Bertrand H., Bouyon A., Mata J., Tappe S. and Day J. M. D. (2020)  
867 Calcium isotopic evidence for the mantle sources of carbonatites. *Science Advances* **6**,  
868 eaba3269.

869 Antonelli M. A. and Simon J. I. (2020) Calcium isotopes in high-temperature terrestrial  
870 processes. *Chem. Geol.* **548**, 119651.

871 Aulbach S., Rudnick R. L. and McDonough W. F. (2011) Evolution of the lithospheric mantle  
872 beneath the East African Rift in Tanzania and its potential signatures in rift magmas. *Geol.*  
873 *Soc. Am. Spec. Pap.* **478**, 105-125.

874 Banerjee A. and Chakrabarti R. (2019) A geochemical and Nd, Sr and stable Ca isotopic study  
875 of carbonatites and associated silicate rocks from the ~65 Ma old Ambadongar carbonatite  
876 complex and the Phenai Mata igneous complex, Gujarat, India: Implications for crustal  
877 contamination, carbonate recycling, hydrothermal alteration and source-mantle mineralogy.  
878 *Lithos* **326-327**, 572-585.

879 Banerjee A., Chakrabarti R. and Simonetti A. (2021) Temporal evolution of  $\delta^{44}\text{Ca}$  and  
880  $^{87}\text{Sr}/^{86}\text{Sr}$  of carbonatites: Implications for crustal recycling through time. *Geochim.*  
881 *Cosmochim. Acta* **307**, 168-191.

882 Blättler C. L. and Higgins J. A. (2017) Testing Urey's carbonate–silicate cycle using the  
883 calcium isotopic composition of sedimentary carbonates. *Earth Planet Sci Lett* **479**, 241-251.

884 Bodinier J.-L., Vasseur G., Vernières J., Dupuy C. and Fabriès J. (1990) Mechanisms of  
885 mantle metasomatism: geochemical evidence from the Lherz orogenic peridotite. *J. Petrol.* **31**,  
886 597-628.

887 Brey G., Brice W. R., Ellis D. J., Green D. H., Harris K. L. and Ryabchikov I. D. (1983)  
888 Pyroxene-carbonate reactions in the upper mantle. *Earth Planet Sci Lett* **62**, 63-74.

889 Carlson R. W. and Ionov D. A. (2019) Compositional characteristics of the MORB mantle and  
890 bulk silicate earth based on spinel peridotites from the Tariat Region, Mongolia. *Geochim.*  
891 *Cosmochim. Acta* **257**, 206-223.

892 Charlier B. L. A., Ginibre C., Morgan D., Nowell G. M., Pearson D. G., Davidson J. P. and  
893 Ottley C. J. (2006) Methods for the microsampling and high-precision analysis of strontium  
894 and rubidium isotopes at single crystal scale for petrological and geochronological  
895 applications. *Chem. Geol.* **232**, 114-133.

896 Chen C., Ciazela J., Li W., Dai W., Wang Z., Foley S. F., Li M., Hu Z. and Liu Y. (2020)

897 Calcium isotopic compositions of oceanic crust at various spreading rates. *Geochim.*  
898 *Cosmochim. Acta* **278**, 272-288.

899 Chen C., Dai W., Wang Z., Liu Y., Li M., Becker H. and Foley S. F. (2019) Calcium isotope  
900 fractionation during magmatic processes in the upper mantle. *Geochim. Cosmochim. Acta* **249**,  
901 121-137.

902 Chen C., Liu Y., Feng L., Foley S. F., Zhou L., Ducea M. N. and Hu Z. (2018) Calcium  
903 isotope evidence for subduction-enriched lithospheric mantle under the northern North China  
904 Craton. *Geochim. Cosmochim. Acta* **238**, 55-67.

905 Choi S. H., Suzuki K., Mukasa S. B., Lee J.-I. and Jung H. (2010) Lu-Hf and Re-Os  
906 systematics of peridotite xenoliths from Spitsbergen, western Svalbard: Implications for  
907 mantle-crust coupling. *Earth Planet Sci Lett* **297**, 121-132.

908 Coltorti M., Bonadiman C., Hinton R. W., Siena F. and Upton B. G. J. (1999) Carbonatite  
909 metasomatism of the oceanic upper mantle: Evidence from clinopyroxenes and glasses in  
910 ultramafic xenoliths of Grande Comore, Indian Ocean. *J. Petrol.* **40**, 133-165.

911 Dai W., Wang Z., Liu Y., Chen C., Zong K., Zhou L., Zhang G., Li M., Moynier F. and Hu Z.  
912 (2020) Calcium isotope compositions of mantle pyroxenites. *Geochimica et Cosmochimica*  
913 *Acta* **270**, 144-159.

914 Dalton J. A. and Wood B. J. (1995) The stability of carbonate under upper-mantle conditions  
915 as a function of temperature and oxygen fugacity. *Eur. J. Miner.* **7**, 883-891.

916 Dautria J. M., Dupuy C., Takherist D. and Dostal J. (1992) Carbonate metasomatism in the  
917 lithospheric mantle: the peridotitic xenoliths from a melilititic district of the Sahara Basin.  
918 *Contrib. Mineral. Petrol.* **111**, 37-52.

919 Deng L., Liu Y., Zong K., Zhu L., Xu R., Hu Z. and Gao S. (2017) Trace element and Sr  
920 isotope records of multi-episode carbonatite metasomatism on the eastern margin of the North  
921 China Craton. *Geochem. Geophys. Geosyst.* **18**, 220-237.

922 DePaolo D. J. (2004) Calcium Isotopic Variations Produced by Biological, Kinetic,  
923 Radiogenic and Nucleosynthetic Processes. *Rev. Mineral. Geochem.* **55**, 255-288.

924 Du L., Long X., Yuan C., Zhang Y., Huang Z., Sun M. and Xiao W. (2018) Petrogenesis of  
925 Late Paleozoic diorites and A-type granites in the central Eastern Tianshan, NW China:  
926 Response to post-collisional extension triggered by slab breakoff. *Lithos* **318-319**, 47-59.

927 Du L., Yuan C., Li X.-P., Zhang Y., Huang Z. and Long X. (2019) Petrogenesis and  
928 Geodynamic Implications of the Carboniferous Granitoids in the Dananhu Belt, Eastern  
929 Tianshan Orogenic Belt. *J. Earth Sci.* **30**, 1243-1252.

930 Fantle M. S. and Tipper E. T. (2014) Calcium isotopes in the global biogeochemical Ca cycle:  
931 Implications for development of a Ca isotope proxy. *Earth-Sci. Rev.* **129**, 148-177.

932 Farkaš J., Böhm F., Wallmann K., Blenkinsop J., Eisenhauer A., van Geldern R., Munnecke  
933 A., Voigt S. and Veizer J. (2007) Calcium isotope record of Phanerozoic oceans: Implications  
934 for chemical evolution of seawater and its causative mechanisms. *Geochim. Cosmochim. Acta*  
935 **71**, 5117-5134.

936 Feng L.-p., Zhou L., Yang L., DePaolo D. J., Tong S.-Y., Liu Y.-S., Owens T. L. and Gao S.  
937 (2017) Calcium Isotopic Compositions of Sixteen USGS Reference Materials. *Geostand.*  
938 *Geoanal. Res.* **41**, 93-106.

939 Fitzpayne A., Giuliani A., Maas R., Hergt J., Janney P. and Phillips D. (2019) Progressive  
940 metasomatism of the mantle by kimberlite melts: Sr–Nd–Hf–Pb isotope compositions of  
941 MARID and PIC minerals. *Earth and Planetary Science Letters* **509**, 15-26.

942 Frezzotti M. L., Andersen T., Neumann E.-R. and Simonsen S. L. (2002) Carbonatite  
943 melt-CO<sub>2</sub> fluid inclusions in mantle xenoliths from Tenerife, Canary Islands: a story of  
944 trapping, immiscibility and fluid-rock interaction in the upper mantle. *Lithos* **64**, 77-96.

945 Green D. H. and Wallace M. E. (1988) Mantle metasomatism by ephemeral carbonatite melts.  
946 *Nature* **336**, 459-462.

947 Griffin W. L., Nikolic N., O'Reilly S. Y. and Pearson N. J. (2012) Coupling, decoupling and  
948 metasomatism: Evolution of crust–mantle relationships beneath NW Spitsbergen. *Lithos* **149**,  
949 115-135.

950 Guo P., Ionov D. A., Xu W.-L., Wang C.-G. and Luan J.-P. (2020) Mantle and recycled  
951 oceanic crustal components in mantle xenoliths from northeastern China and their mantle  
952 sources. *J. Geophys. Res. Solid Earth* **125**, e2019JB018232.

953 Hauri E. H., Shimizu N., Dieu J. J. and Hart S. R. (1993) Evidence for hotspot-related  
954 carbonatite metasomatism in the oceanic upper mantle. *Nature* **365**, 221-227.

955 He Y., Wang Y., Zhu C., Huang S. and Li S. (2017) Mass-Independent and Mass-Dependent  
956 Ca Isotopic Compositions of Thirteen Geological Reference Materials Measured by Thermal  
957 Ionisation Mass Spectrometry. *Geostand. Geoanal. Res.* **41**, 283-302.

958 Herzberg C. (2004) Geodynamic information in peridotite petrology. *J. Petrol.* **45**, 2507-2530.

959 Heuser A., Eisenhauer A., Gussone N., Bock B., Hansen B. T. and Nägler T. F. (2002)  
960 Measurement of calcium isotopes ( $\delta^{44}\text{Ca}$ ) using a multicollector TIMS technique. *Int. J.*  
961 *Mass Spectrom.* **220**, 385-397.

962 Hofmann A. W. (1988) Chemical differentiation of the Earth: the relationship between mantle,  
963 continental crust, and oceanic crust. *Earth Planet Sci Lett* **90**, 297-314.

964 Hofmann A. W. (1997) Mantle geochemistry: the message from oceanic volcanism. *Nature*  
965 **385**, 219-229.

966 Hofmann A. W. (2003) Sampling mantle heterogeneity through oceanic basalts: isotopes and  
967 trace elements, in: Carlson, R.W. (Ed.), *Treatise on Geochemistry*. Vol. 2. The Mantle and  
968 Core. Elsevier, pp. 61-102.

969 Howarth G. H., Moore A. E., Harris C., van der Meer Q. H. A. and le Roux P. (2019) Crustal  
970 versus mantle origin of carbonate xenoliths from Kimberley region kimberlites using  
971 C-O-Sr-Nd-Pb isotopes and trace element abundances. *Geochimica et Cosmochimica Acta*  
972 **266**, 258-273.

973 Huang S., Farkas J. and Jacobsen S. B. (2010) Calcium isotopic fractionation between  
974 clinopyroxene and orthopyroxene from mantle peridotites. *Earth Planet Sci Lett* **292**,  
975 337-344.

976 Huang S., Farkaš J. and Jacobsen S. B. (2011) Stable calcium isotopic compositions of  
977 Hawaiian shield lavas: Evidence for recycling of ancient marine carbonates into the mantle.  
978 *Geochim. Cosmochim. Acta* **75**, 4987-4997.

979 Ionov D. and Harmer R. E. (2002) Trace element distribution in calcite-dolomite carbonatites  
980 from Spitskop: inferences for differentiation of carbonatite magmas and the origin of

981 carbonates in mantle xenoliths. *Earth and Planetary Science Letters* **198**, 495-510.

982 Ionov D. A. (1998) Trace element composition of mantle-derived carbonates and coexisting  
983 phases in peridotite xenoliths from alkali basalts. *J. Petrol.* **39**, 1931-1941.

984 Ionov D. A. (2007) Compositional variations and heterogeneity in fertile lithospheric mantle:  
985 peridotite xenoliths in basalts from Tariat, Mongolia. *Contrib. Mineral. Petrol.* **154**, 455-477.

986 Ionov D. A., Bodinier J.-L., Mukasa S. B. and Zanetti A. (2002a) Mechanisms and sources of  
987 mantle metasomatism: major and trace element compositions of peridotite xenoliths from  
988 Spitsbergen in the context of numerical modeling. *J. Petrol.* **43**, 2219-2259.

989 Ionov D. A., Doucet L. S., Pogge von Strandmann P. A. E., Golovin A. V. and Korsakov A. V.  
990 (2017) Links between deformation, chemical enrichments and Li-isotope compositions in the  
991 lithospheric mantle of the central Siberian craton. *Chem. Geol.* **475**, 105-121.

992 Ionov D. A., Doucet L. S., Xu Y., Golovin A. V. and Oleinikov O. B. (2018) Reworking of  
993 Archean mantle in the NE Siberian craton by carbonatite and silicate melt metasomatism:  
994 Evidence from a carbonate-bearing, dunite-to-websterite xenolith suite from the  
995 Obnazhennaya kimberlite. *Geochimica et Cosmochimica Acta* **224**, 132-153.

996 Ionov D. A., Dupuy C., O'Reilly S. Y., Kopylova M. G. and Genshaft Y. S. (1993) Carbonated  
997 peridotite xenoliths from Spitsbergen: implications for trace element signature of mantle  
998 carbonate metasomatism. *Earth Planet Sci Lett* **119**, 283-297.

999 Ionov D. A. and Hofmann A. W. (2007) Depth of formation of sub-continental off-craton  
1000 peridotites. *Earth Planet Sci Lett* **261**, 620-634.

1001 Ionov D. A., Hofmann A. W. and Shimizu N. (1994) Metasomatism-induced melting in  
1002 mantle xenoliths from Mongolia. *J. Petrol.* **35**, 753-785.

1003 Ionov D. A., Mukasa S. B. and Bodinier J.-L. (2002b) Sr-Nd-Pb isotopic compositions of  
1004 peridotite xenoliths from Spitsbergen: numerical modelling indicates Sr-Nd decoupling in the  
1005 mantle by melt percolation metasomatism. *J. Petrol.* **43**, 2261-2278.

1006 Ionov D. A., O'Reilly S. Y., Kopylova M. G. and Genshaft Y. S. (1996) Carbonate-bearing  
1007 mantle peridotite xenoliths from Spitsbergen: phase relationships, mineral compositions and  
1008 trace element residence. *Contrib. Mineral. Petrol.* **125**, 375-392.

1009 Ionov D. A., Qi Y.-H., Kang J.-T., Golovin A. V., Oleinikov O. B., Zheng W., Anbar A. D.,  
1010 Zhang Z.-F. and Huang F. (2019) Calcium isotopic signatures of carbonatite and silicate  
1011 metasomatism, melt percolation and crustal recycling in the lithospheric mantle. *Geochim.  
1012 Cosmochim. Acta* **248**, 1-13.

1013 Ionov D. A., Shirey S. B., Weis D. and Brügmann G. (2006) Os-Hf-Sr-Nd isotope and PGE  
1014 systematics of spinel peridotite xenoliths from Tok, SE Siberian craton: Effects of pervasive  
1015 metasomatism in shallow refractory mantle. *Earth Planet Sci Lett* **241**, 47-64.

1016 Kang J.-T., Ionov D. A., Liu F., Zhang C.-L., Golovin A. V., Qin L.-P., Zhang Z.-F. and Huang  
1017 F. (2017) Calcium isotopic fractionation in mantle peridotites by melting and metasomatism  
1018 and Ca isotope composition of the Bulk Silicate Earth. *Earth Planet Sci Lett* **474**, 128-137.

1019 Kang J.-T., Ionov D. A., Zhu H.-L., Liu F., Zhang Z.-F., Liu Z. and Huang F. (2019) Calcium  
1020 isotope sources and fractionation during melt-rock interaction in the lithospheric mantle:  
1021 Evidence from pyroxenites, wehrlites, and eclogites. *Chem. Geol.* **524**, 272-282.

1022 Kang J.-T., Zhou C., Huang J.-Y., Hao Y.-T., Liu F., Zhu H.-L., Zhang Z.-F. and Huang F.

1023 (2020) Diffusion-driven Ca-Fe isotope fractionations in the upper mantle: Implications for  
1024 mantle cooling and melt infiltration. *Geochim. Cosmochim. Acta* **290**, 41-58.

1025 Kang J.-T., Zhu H.-L., Liu Y.-F., Liu F., Wu F., Hao Y.-T., Zhi X.-C., Zhang Z.-F. and Huang F.  
1026 (2016) Calcium isotopic composition of mantle xenoliths and minerals from Eastern China.  
1027 *Geochim. Cosmochim. Acta* **174**, 335-344.

1028 Katayama I., Suyama Y., Ando J.-i. and Komiya T. (2009) Mineral chemistry and P-T  
1029 condition of granular and sheared peridotite xenoliths from Kimberley, South Africa: Origin  
1030 of the textural variation in the cratonic mantle. *Lithos* **109**, 333-340.

1031 Kramers J. D., Roddick J. C. M. and Dawson J. B. (1983) Trace element and isotope studies  
1032 on veined, metasomatic and “MARID” xenoliths from Bultfontein, South Africa. *Earth  
1033 Planet Sci Lett* **65**, 90-106.

1034 Laurora A., Mazzucchelli M., Rivalenti G., Vannucci R., Zanetti A., Barbieri M. A. and  
1035 Cingolani C. A. (2001) Metasomatism and melting in carbonated peridotite xenoliths from the  
1036 mantle wedge: The Gobernador Gregores case (southern Patagonia). *J. Petrol.* **42**, 69-87.

1037 Li C. F., Li X. H., Li Q. L., Guo J. H., Li X. H. and Yang Y. H. (2012) Rapid and precise  
1038 determination of Sr and Nd isotopic ratios in geological samples from the same filament  
1039 loading by thermal ionization mass spectrometry employing a single-step separation scheme.  
1040 *Anal Chim Acta* **727**, 54-60.

1041 Liu F., Li X., Wang G., Liu Y., Zhu H., Kang J., Huang F., Sun W., Xia X. and Zhang Z.  
1042 (2017a) Marine carbonate component in the mantle beneath the southeastern Tibetan Plateau:  
1043 evidence from magnesium and calcium isotopes. *J. Geophys. Res. Solid Earth* **122**,  
1044 9729-9744.

1045 Liu F., Zhu H. L., Li X., Wang G. Q. and Zhang Z. F. (2017b) Calcium Isotopic Fractionation  
1046 and Compositions of Geochemical Reference Materials. *Geostand Geoanal Res* **41**, 675-688.

1047 Liu J., Carlson R. W., Rudnick R. L., Walker R. J., Gao S. and Wu F.-y. (2012) Comparative  
1048 Sr–Nd–Hf–Os–Pb isotope systematics of xenolithic peridotites from Yangyuan, North China  
1049 Craton: Additional evidence for a Paleoproterozoic age. *Chem Geol* **332–333**, 1-14.

1050 Luo Y., Qin H., Wu T. and Li Z. (2020) Petrogenesis of the Granites in the Yandangshan Area,  
1051 Southeastern China: Constraints from SHRIMP U-Pb Zircon Age and Trace Elements, and  
1052 Sr-Nd-Hf Isotopic Data. *J. Earth Sci.* **31**, 693-708.

1053 Ma J., Wei G., Liu Y., Ren Z., Xu Y. and Yang Y. (2013) Precise measurement of stable  
1054 neodymium isotopes of geological materials by using MC-ICP-MS. *JAAS* **28**, 1926-1931.

1055 McDonough W. F. and Sun S.-s. (1995) The composition of the Earth. *Chem Geol* **120**,  
1056 223-253.

1057 Meng F., Xu W., Xu Q., Guo J. and Zhang Y. (2019) Decoupling of Lu-Hf and Sm-Nd  
1058 Isotopic System in Deep-Seated Xenoliths from the Xuzhou-Suzhou Area, China: Differences  
1059 in Element Mobility during Metamorphism. *J. Earth Sci.* **30**, 1266-1279.

1060 Navon O. and Stolper E. (1987) Geochemical consequences of melt percolation: the upper  
1061 mantle as a chromatographic column. *Journal of Geology* **95**, 285-307.

1062 Pearson D. G., Canil D. and Shirey S. B. (2014) Mantle samples included in volcanic rocks:  
1063 Xenoliths and diamonds, in: Carlson, R.W. (Ed.), *Treatise on Geochemistry* (Second Edition).  
1064 Elsevier, Oxford, pp. 169-253.

1065 Rivalenti G., Zanetti A., Mazzucchelli M., Vannucci R. and Cingolani C. A. (2004) Equivocal  
1066 carbonatite markers in the mantle xenoliths of the Patagonia backarc: the Gobernador  
1067 Gregores case (Santa Cruz Province, Argentina). *Contrib. Mineral. Petrol.* **147**, 647-670.

1068 Rudnick R. L., McDonough W. F. and Chappell B. C. (1993) Carbonatite metasomatism in  
1069 the northern Tanzanian mantle. *Earth Planet Sci Lett* **114**, 463-475.

1070 Skulan J., DePaolo D. J. and Owens T. L. (1997) Biological control of calcium isotopic  
1071 abundances in the global calcium cycle. *Geochim. Cosmochim. Acta* **61**, 2505-2510.

1072 Stracke A. (2012) Earth's heterogeneous mantle: A product of convection-driven interaction  
1073 between crust and mantle. *Chem Geol* **330–331**, 274-299.

1074 Streckeisen A. (1976) To each plutonic rock its proper name. *Earth Sci. Rev.* **12**, 1-33.

1075 Sun J., Zhu X. K., Belshaw N. S., Chen W., Doroshkevich A. G., Luo W. J., Song W. L., Chen  
1076 B. B., Cheng Z. G., Li Z. H., Wang Y., Kynicky J. and Henderson G. M. (2021) Ca isotope  
1077 systematics of carbonatites: Insights into carbonatite source and evolution. *Geochemical  
1078 Perspectives Letters* **17**, 11-15.

1079 Tanaka T., Togashi S., Kamioka H., Amakawa H., Kagami H., Hamamoto T., Yuhara M.,  
1080 Orihashi Y., Yoneda S., Shimizu H., Kunimaru T., Takahashi K., Yanagi T., Nakano T.,  
1081 Fujimaki H., Shinjo R., Asahara Y., Tanimizu M. and Dragusanu C. (2000) JNdi-1: a  
1082 neodymium isotopic reference in consistency with LaJolla neodymium. *Chem Geol* **168**,  
1083 279-281.

1084 Tang W., Hui H., Ionov D. A., Chen W., Zhang L. and Xu Y. (2020) Metasomatism-controlled  
1085 hydrogen distribution in the Spitsbergen upper mantle. *Am. Mineral.* **105**, 1326-1341.

1086 Tappe S., Romer R. L., Stracke A., Steenfelt A., Smart K. A., Muehlenbachs K. and Torsvik T.  
1087 H. (2017) Sources and mobility of carbonate melts beneath cratons, with implications for  
1088 deep carbon cycling, metasomatism and rift initiation. *Earth Planet Sci Lett* **466**, 152-167.

1089 Tappe S., Stracke A., van Acken D., Strauss H. and Luguet A. (2020) Origins of kimberlites  
1090 and carbonatites during continental collision – Insights beyond decoupled Nd-Hf isotopes.  
1091 *Earth-Science Reviews* **208**, 103287.

1092 Thirlwall M. F. (1991) Long-term reproducibility of multicollector Sr and Nd isotope ratio  
1093 analysis. *Chem. Geol.* **94**, 85-104.

1094 Vagnes E. and Amundsen H. E. F. (1993) Late Cenozoic uplift and volcanism on Spitsbergen:  
1095 Caused by mantle convection? *Geology* **21**, 251-254.

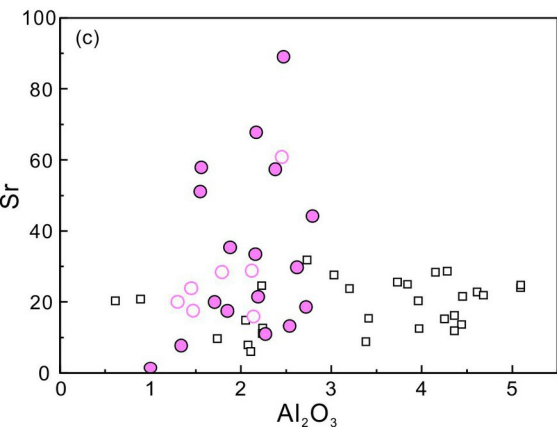
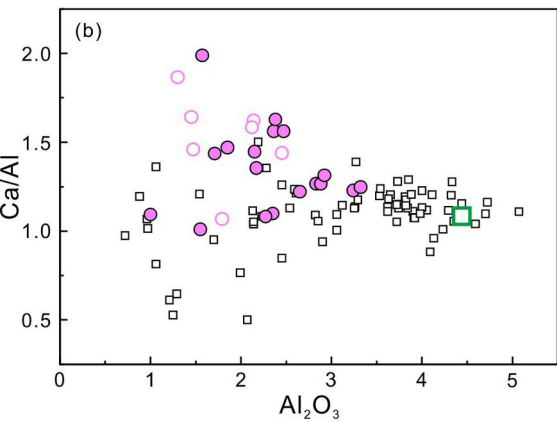
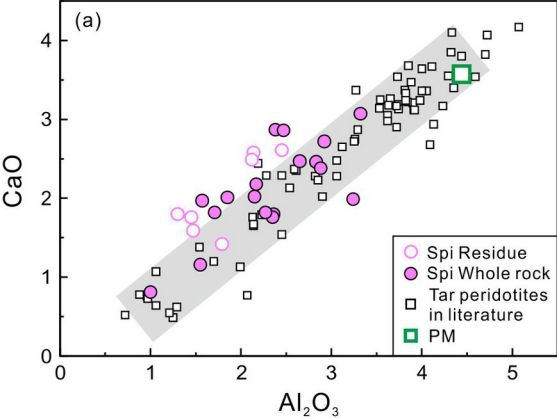
1096 Valdes M. C., Moreira M., Foriel J. and Moynier F. (2014) The nature of Earth's building  
1097 blocks as revealed by calcium isotopes. *Earth Planet Sci Lett* **394**, 135-145.

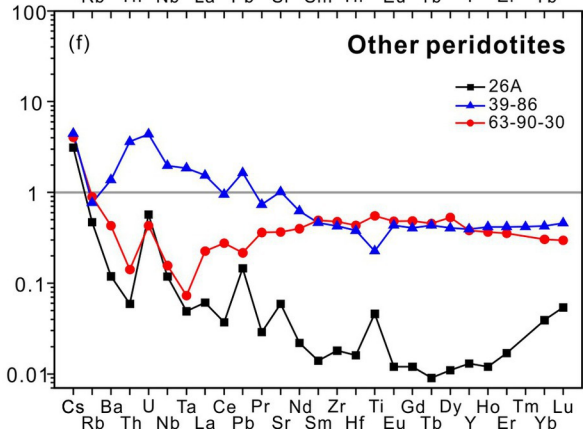
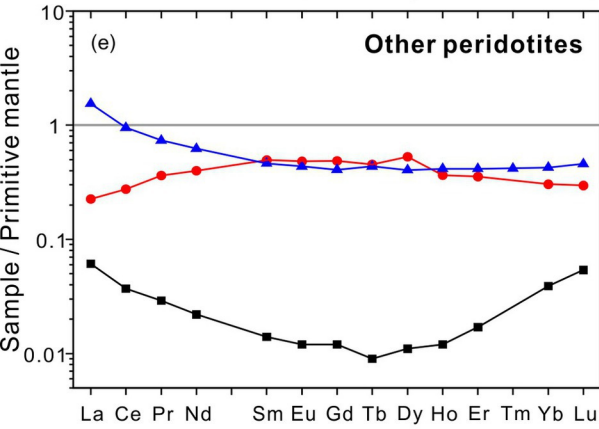
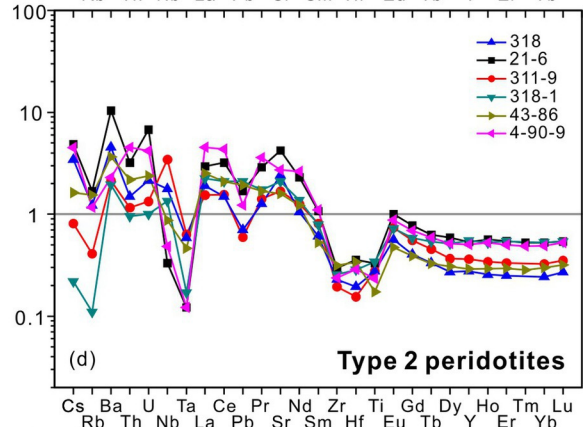
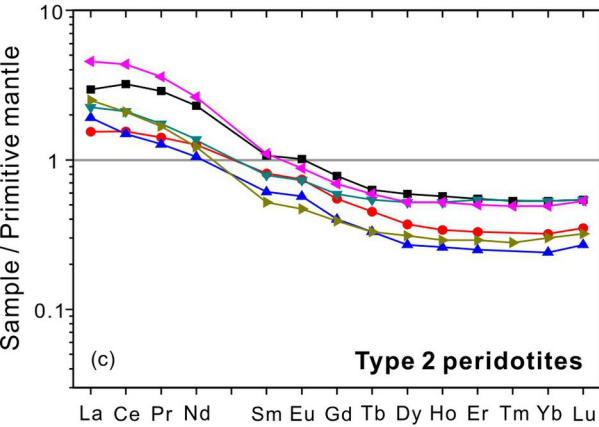
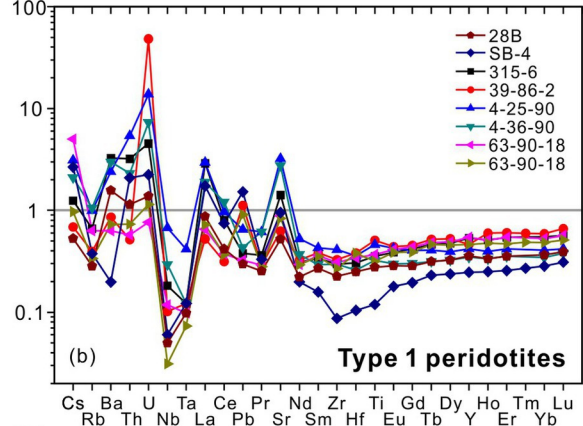
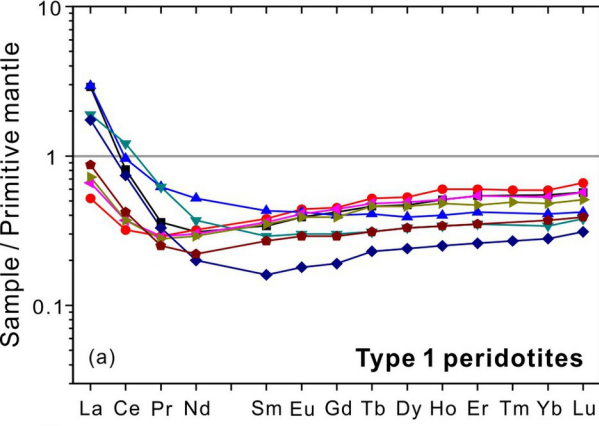
1098 van der Meer Q. H. A., Klaver M., Waight T. E. and Davies G. R. (2013) The provenance of  
1099 sub-cratonic mantle beneath the Limpopo Mobile Belt (South Africa). *Lithos* **170–171**,  
1100 90-104.

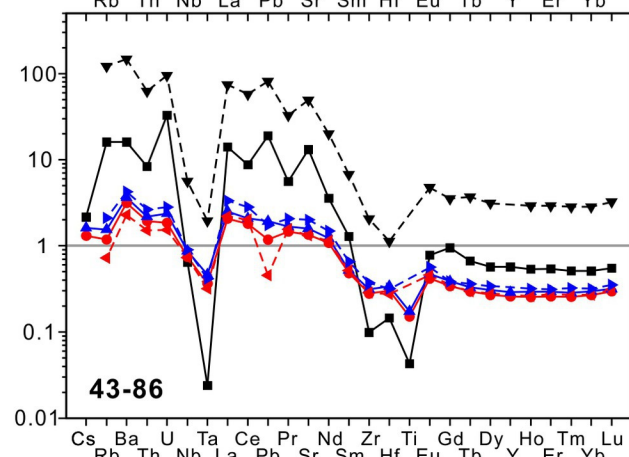
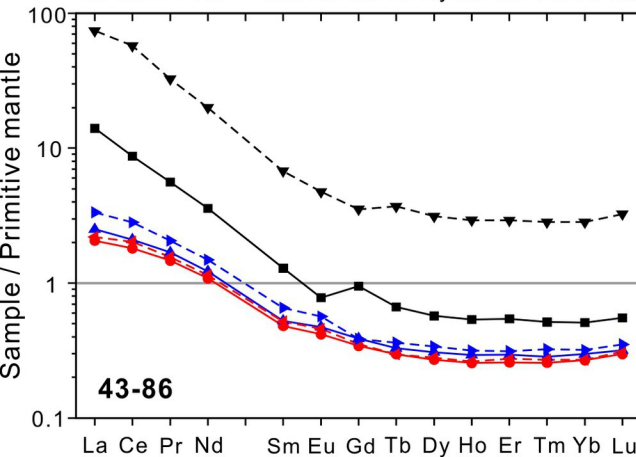
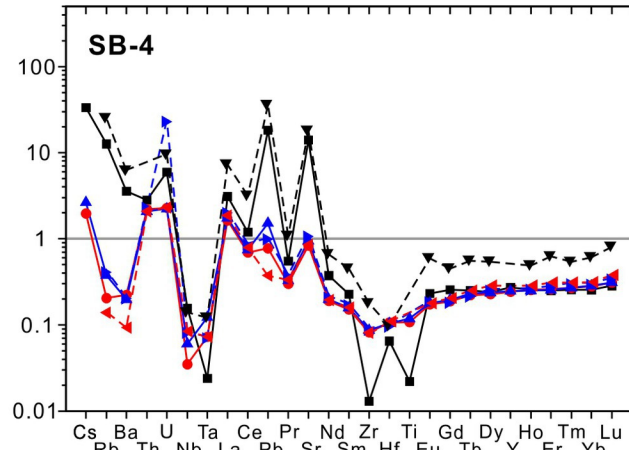
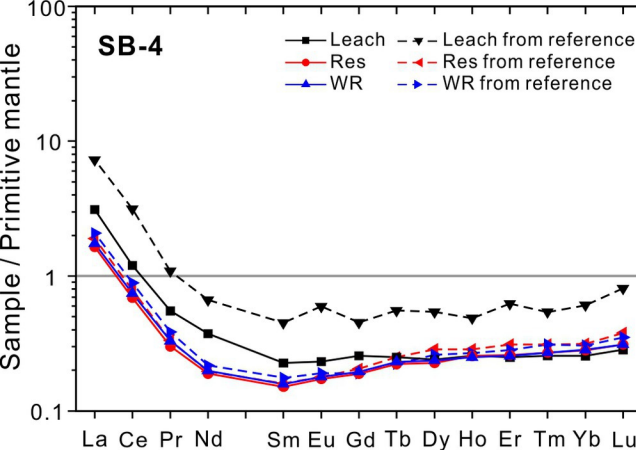
1101 Wang Z., Ma J., Li J., Wei G., Zeng T., Li L., Zhang L., Deng W., Xie L. and Liu Z. (2018) Fe  
1102 (hydro) oxide controls Mo isotope fractionation during the weathering of granite. *Geochim.  
1103 Cosmochim. Acta* **226**, 1-17.

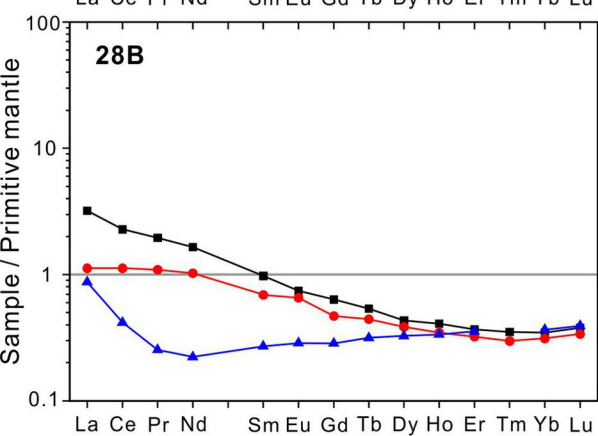
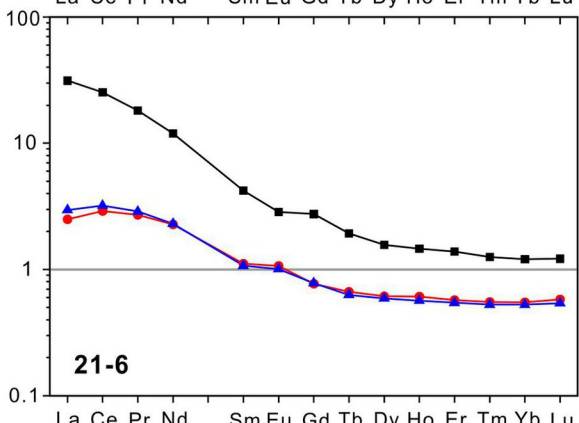
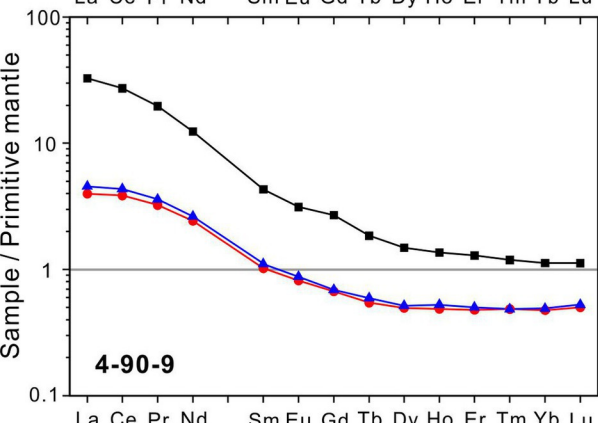
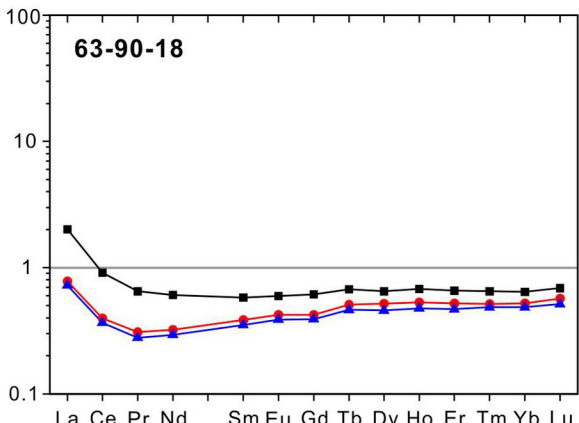
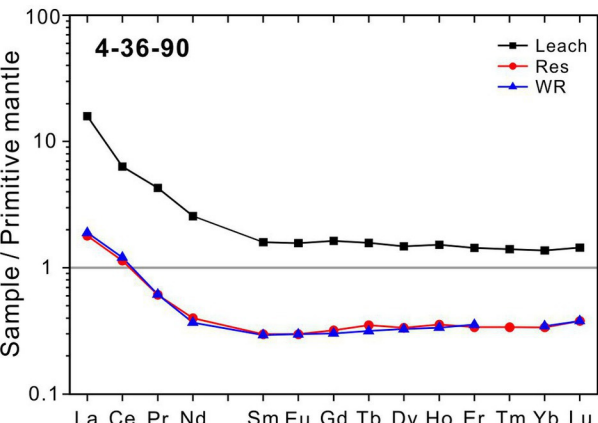
1104 Weis D., Kieffer B., Maerschalk C., Barling J., de Jong J., Williams G. A., Hanano D.,  
1105 Pretorius W., Mattielli N., Scoates J. S., Goolaerts A., Friedman R. M. and Mahoney J. B.  
1106 (2006) High-precision isotopic characterization of USGS reference materials by TIMS and

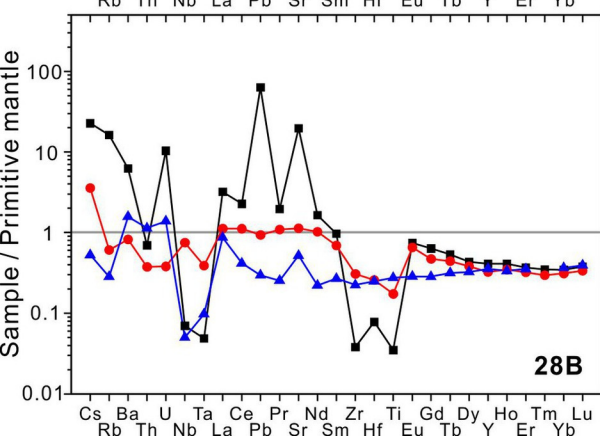
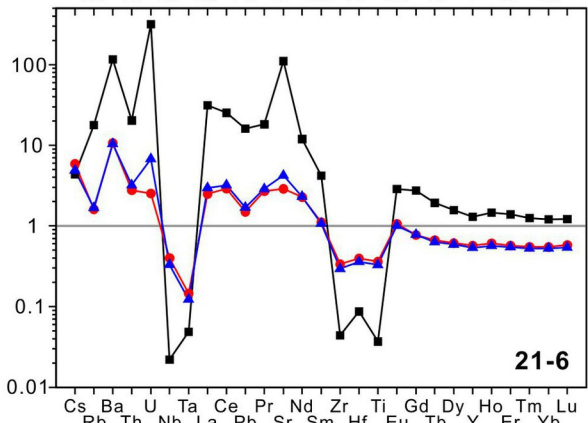
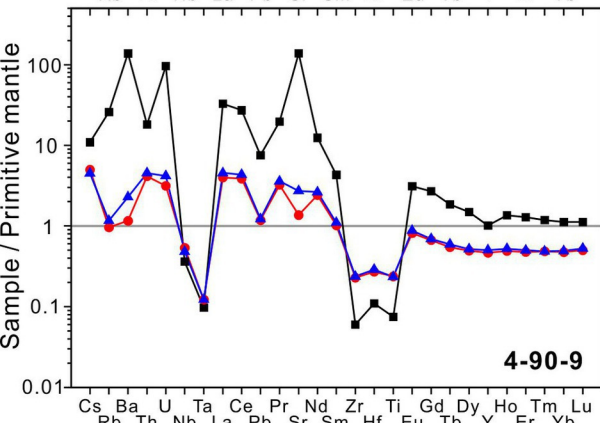
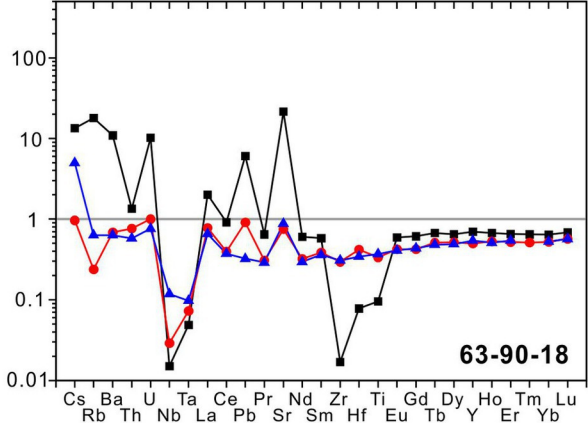
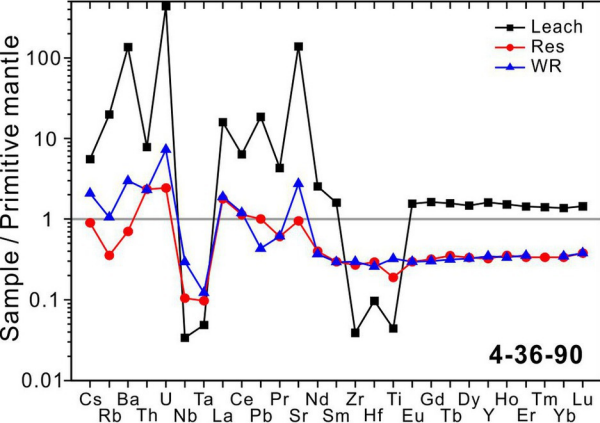
1107 MC-ICP-MS. *Geochem. Geophys. Geosyst.* **7**.  
1108 Workman R. K. and Hart S. R. (2005) Major and trace element composition of the depleted  
1109 MORB mantle (DMM). *Earth Planet Sci Lett* **231**, 53-72.  
1110 Xu M., Jing Z., Bajgain S. K., Mookherjee M., Van Orman J. A., Yu T. and Wang Y. (2020)  
1111 High-pressure elastic properties of dolomite melt supporting carbonate-induced melting in  
1112 deep upper mantle. *Proc. Natl. Acad. Sci. USA*, 202004347.  
1113 Xu Y. (2002) Evidence for crustal components in the mantle and constraints on crustal  
1114 recycling mechanisms: pyroxenite xenoliths from Hannuoba, North China. *Chem. Geol.* **182**,  
1115 301-322.  
1116 Yaxley G. M., Crawford A. J. and Green D. H. (1991) Evidence for carbonatite metasomatism  
1117 in spinel peridotite xenoliths from western Victoria, Australia. *Earth Planet Sci Lett* **107**,  
1118 305-317.  
1119 Yaxley G. M., Green D. H. and Kamenetsky V. (1998) Carbonate metasomatism in the  
1120 southeastern Australian lithosphere. *J. Petrol.* **39**, 1917-1931.  
1121 Zhao X., Zhang Z., Huang S., Liu Y., Li X. and Zhang H. (2017) Coupled extremely light Ca  
1122 and Fe isotopes in peridotites. *Geochim. Cosmochim. Acta* **208**, 368-380.  
1123 Zhu H., Du L., Li X., Zhang Z. and Sun W. (2020) Calcium isotopic fractionation during plate  
1124 subduction: Constraints from back-arc basin basalts. *Geochim. Cosmochim. Acta* **270**,  
1125 379-393.  
1126 Zhu H., Liu F., Li X., An Y., Wang G. and Zhang Z. (2018a) A “peak cut” procedure of  
1127 column separation for calcium isotope measurement using the double spike technique and  
1128 thermal ionization mass spectrometry (TIMS). *J. Anal. At. Spectrom.* **33**, 547-554.  
1129 Zhu H., Liu F., Li X., Wang G., Zhang Z. and Sun W. (2018b) Calcium isotopic compositions  
1130 of normal Mid-Ocean Ridge basalts from the southern Juan de Fuca Ridge. *J. Geophys. Res.*  
1131 *Solid Earth* **123**, 1303-1313.  
1132 Zhu H. L., Zhang Z. F., Wang G. Q., Liu Y. F., Liu F., Li X. and Sun W. D. (2016) Calcium  
1133 Isotopic Fractionation during Ion-Exchange Column Chemistry and Thermal Ionisation Mass  
1134 Spectrometry (TIMS) Determination. *Geostand. Geoanal. Res.* **40**, 185-194.  
1135

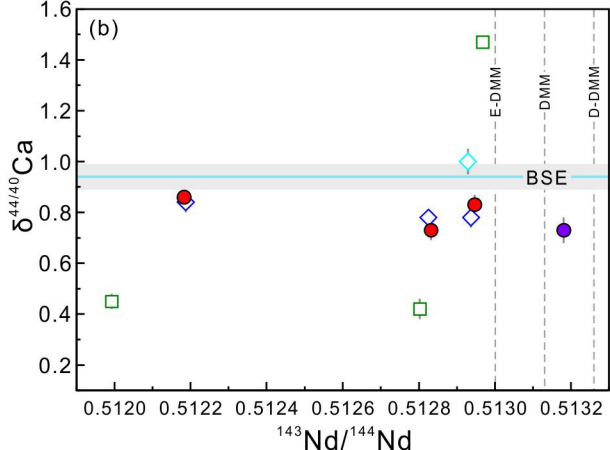
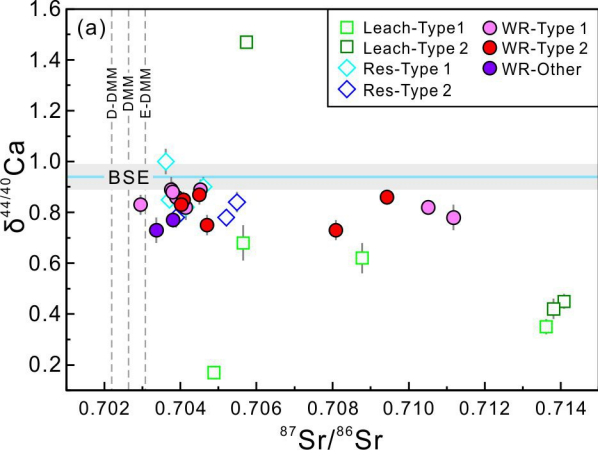


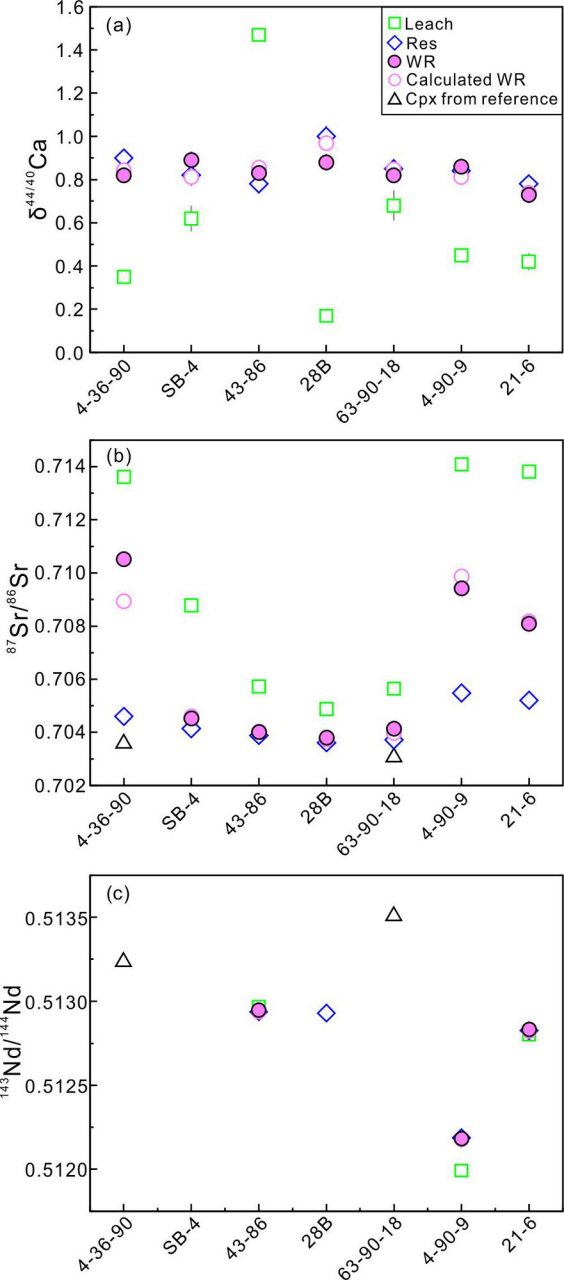


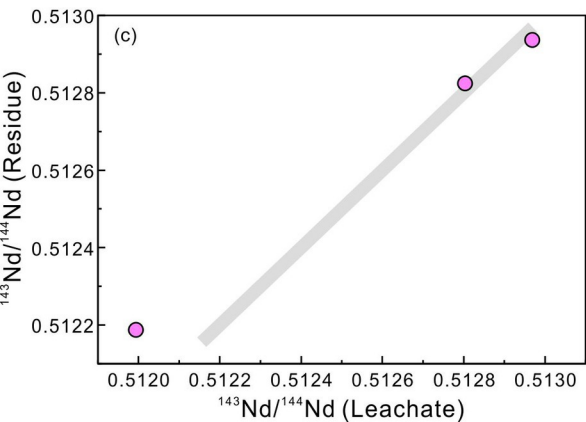
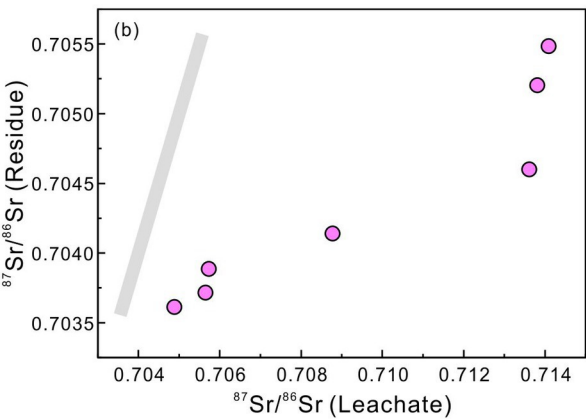
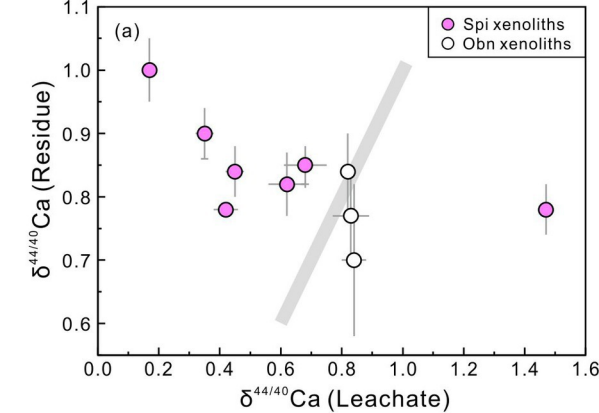












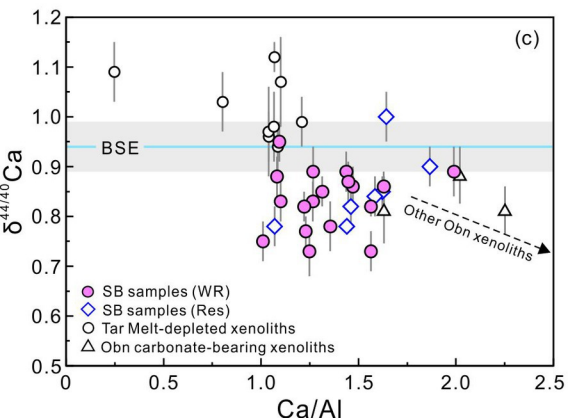
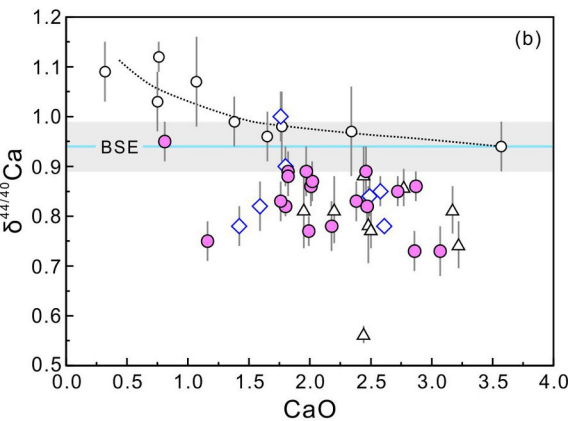
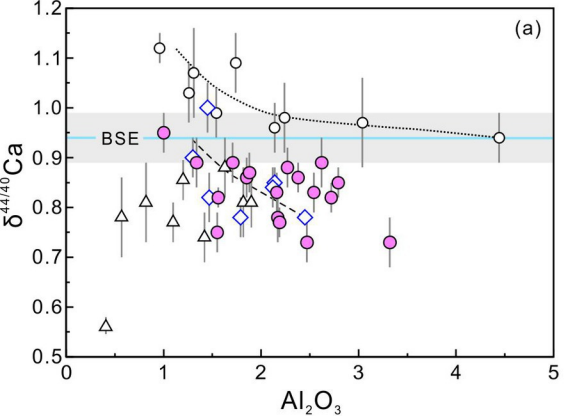


Table 1. Sample list and information summary for the Spitsbergen xenoliths.

Sample	Location	Rock type <sup>a</sup>	Leaching	Data source <sup>b</sup>														
				Major elements			Trace elements			Sr isotopes			Nd isotopes			Ca isotopes		
				WR	Res	Leach	WR	Res	Leach	WR	Res	Leach	WR	Res	Leach	WR	Res	Leach
4-36-90*	Halvdan	Spl Lh	×	×	×	×	(2)	×	×	×	×	×	×	×	×	×	×	×
4-90-9*	Halvdan	Spl Lh	×	×	×	×	×	×	×	×	×	×	×	×	×	×	×	×
21-6*	Halvdan	Spl Lh	×	×	×	×	×	×	×	×	×	×	×	×	×	×	×	×
43-86*	Sverre	Spl Lh	×	×	×	×	×	×	×	×	×	×	×	×	×	×	×	×
28B	Sverre	Spl Lh	×	(3)	×	×	(2)	×	×	×	×	×	×	×	×	×	×	×
63-90-18	Sverre	Spl Lh	×	×	×	×	(2)	×	×	×	×	×	×	×	×	×	×	×
SB-4	Halvdan	Spl Lh	×	×	×	×	×	×	×	×	×	×	×	×	×	×	×	×
315-6	Halvdan	Spl Lh		×			(2)			×							×	
39-86-2	Sverre	Spl Lh		×			(2)			×							×	
4-25-90	Halvdan	Spl Lh		(2)			(2)			×							×	
63-90-18-1	Sverre	Spl Lh		×			×			×							×	
311-9	Halvdan	Spl Lh		×			(2)			×							×	
318	Halvdan	H <sub>z</sub>		(2)			(2)			×							×	
318-1	Halvdan	Spl Lh		×			(2)			×							×	
26A	Sverre	H <sub>z</sub>		(2)			(2)										×	
63-90-30	Sverre	Spl Lh		×			(2)										×	
39-86	Sverre	Spl Lh		×			×			×							×	
4A-90-1-Cpx	Sigurd	Amph Wh								(4)			(4)				×	
4A-90-1-Amph	Sigurd	Amph Wh								(4)			(4)				×	

<sup>a</sup> Abbreviations: Spl Lh, spinel lherzolite; H<sub>z</sub>, harzburgite; Wh, wehrlite; Cpx, clinopyroxene; Amph, amphibole; WR, whole-rock; Res, residues; Leach, leachates. \*Samples that contain the largest and most abundant carbonate aggregates.

<sup>b</sup> Data sources: ×, this study; (1) [Ionov et al. \(1993\)](#); (2) [Ionov et al. \(2002a\)](#); (3) [Ionov et al. \(1996\)](#); (4) [Ionov et al. \(2002b\)](#).

Table 2. Ca-Sr-Nd isotopic compositions of reference samples.

		$\delta^{44/40}\text{Ca}$	2SD <sup>a</sup>	n <sup>b</sup>	$^{87}\text{Sr}/^{86}\text{Sr}$	2SD	n	$^{143}\text{Nd}/^{144}\text{Nd}$	2SD	n
NIST SRM 915a	This study	-0.02	0.12	21						
	<a href="#">Huang et al. (2010)</a>	0.04	0.13	45						
	<a href="#">Valdes et al. (2014)</a>	0.00	0.17	74						
IAPSO seawater	This study	1.82	0.10	10						
	<a href="#">Farkaš et al. (2007)</a>	1.86	0.20	5						
	<a href="#">He et al. (2017)</a>	1.89	0.18	147						
DTS-1	This study	1.61	0.09	3						
	<a href="#">Huang et al. (2010)</a>	1.59	0.16	3						
	<a href="#">Feng et al. (2017)</a>	1.51	0.13	7						
DTS-2	This study	1.10	0.11	3						
	<a href="#">Feng et al. (2017)</a>	1.20	0.11	9						
PCC-1	This study	1.10	0.08	3						
	<a href="#">Amini et al. (2009)</a>	1.15	0.09	13						
BHVO-2	This study	0.84	0.09	5	0.703503		1			
	<a href="#">Valdes et al. (2014)</a>	0.87	0.16	10						
	<a href="#">He et al. (2017)</a>	0.79	0.09	7						
	<a href="#">Weis et al. (2006)</a>				0.703487	0.000019	12			
NBS-987	This study				0.710254	0.000014	12			
	<a href="#">Thirlwall (1991)</a>				0.710248	0.000011	427			
	<a href="#">Charlier et al. (2006)</a>				0.710255	0.000018	222			
JNdi-1	This study							0.512111	0.000013	14
	<a href="#">Tanaka et al. (2000)</a>							0.512115	0.000007	
	<a href="#">Li et al. (2012)</a>							0.512113	0.000012	5
W-2	This study							0.512512		1
	<a href="#">Li et al. (2012)</a>							0.512518	0.000006	2

<sup>a</sup> 2SD: two standard deviations.

<sup>b</sup> n: number of replicate Ca-Sr-Nd isotope analyses.

Table 3. Ca-Sr-Nd isotopic compositions of leachates, residues, whole-rocks (WR) and calculated WR for carbonate-bearing xenoliths.

Sample		Mass fraction	Ca fraction	$\delta^{44/40}\text{Ca}$	2SD	2SE <sup>a</sup>	n	Sr fraction	$^{87}\text{Sr}/^{86}\text{Sr}^c$	Nd fraction	$^{143}\text{Nd}/^{144}\text{Nd}^c$
4-36-90	Leachate	0.006	0.10	0.35	0.05	0.03	3	0.48	0.713612	0.04	
	Residue	0.994	0.90	0.90	0.07	0.04	3	0.52	0.704601	0.96	
	Whole Rock	1.000	1.00	0.82	0.03	0.02	3	1.00	0.710515	1.00	
	Calculated WR			0.84					0.708932		
4-90-9	Leachate	0.010	0.08	0.45	0.05	0.03	3	0.51	0.714085	0.05	0.511993
	Residue	0.990	0.92	0.84	0.08	0.04	3	0.49	0.705484	0.95	0.512187
	Whole Rock	1.000	1.00	0.86	0.06	0.03	3	1.00	0.709426	1.00	0.512183
	Calculated WR			0.81					0.709869		0.512178
21-6	Leachate	0.014	0.12	0.42	0.07	0.04	3	0.35	0.713810	0.07	0.512803
	Residue	0.986	0.88	0.78	0.02	0.01	3	0.65	0.705203	0.93	0.512825
	Whole Rock	1.000	1.00	0.73	0.06	0.04	3	1.00	0.708086	1.00	0.512832
	Calculated WR			0.74					0.708175		0.512823
43-86	Leachate	0.009	0.11	1.47	0.03	0.02	3	0.08	0.705733	0.03	0.512968
	Leachate-R <sup>b</sup>			1.46	0.08	0.05	3				
	Residue	0.991	0.89	0.78	0.09	0.04	4	0.92	0.703886	0.97	0.512937
	Whole Rock	1.000	1.00	0.85	0.13	0.07	3	1.00	0.704016	1.00	0.512938
	Whole Rock-R <sup>b</sup>			0.82			2		0.704023		0.512956
Calculated WR			0.86					0.704029		0.512938	
SB-4	Leachate	0.007	0.03	0.62	0.10	0.06	3	0.10	0.708775	0.01	
	Residue	0.993	0.97	0.82	0.09	0.05	3	0.90	0.704142	0.99	
	Whole Rock	1.000	1.00	0.89	0.06	0.04	3	1.00	0.704527	1.00	
	Calculated WR			0.81					0.704604		
28B	Leachate	0.006	0.04	0.17	0.02	0.01	3	0.10	0.704880	0.01	
	Residue	0.994	0.96	1.00	0.09	0.05	3	0.90	0.703615	0.99	0.512929
	Whole Rock	1.000	1.00	0.88	0.06	0.04	3	1.00	0.703799	1.00	
	Calculated WR			0.97					0.703742		
63-90-18	Leachate	0.006	0.03	0.68	0.11	0.07	3	0.14	0.705647	0.01	
	Residue	0.994	0.97	0.85	0.05	0.03	3	0.86	0.703716	0.99	
	Whole Rock	1.000	1.00	0.83	0.05	0.03	3	1.00	0.704138	1.00	
	Whole Rock-R <sup>b</sup>			0.80			1		0.704133		
	Calculated WR			0.85					0.703980		

<sup>a</sup> 2SE: two standard deviations of the mean.  $2SE = 2SD/\sqrt{n}$ .

<sup>b</sup> R: repeated dissolution and analysis for two whole rocks and a repeated analysis for one leachate.

<sup>c</sup> Sr-Nd isotopes of leachate, residue and whole rock of carbonate-bearing xenoliths are measured once.

Table 4. Ca-Sr-Nd isotopic compositions of non-leached whole-rock Spitsbergen xenoliths and minerals.

Sample		$\delta^{44/40}\text{Ca}$	2SD	2SE	n	$^{87}\text{Sr}/^{86}\text{Sr}^{\text{a}}$	$^{143}\text{Nd}/^{144}\text{Nd}$
315-6	Whole rock	0.89	0.09	0.05	3	0.703760	
39-86-2	Whole rock	0.83	0.07	0.04	3	0.702950	
4-25-90	Whole rock	0.78	0.12	0.05	7	0.711183	
63-90-18-1	Whole rock	0.86	0.08	0.04	3	0.703893	
311-9	Whole rock	0.87	0.06	0.04	3	0.704491	
318	Whole rock	0.75	0.06	0.04	3	0.704696	
318-1	Whole rock	0.85	0.05	0.03	3	0.704079	
26A	Whole rock	0.95	0.07	0.04	3		
63-90-30	Whole rock	0.89	0.08	0.05	3		
39-86	Whole rock	0.77	0.06	0.03	3	0.703805	
4A-90-1-Cpx <sup>b</sup>	Cpx mineral	1.05	0.09	0.05	3	0.703950 <sup>c</sup>	0.512904 <sup>c</sup>
4A-90-1-Amph <sup>b</sup>	Amph mineral	0.97	0.09	0.05	3	0.704000 <sup>c</sup>	0.512894 <sup>c</sup>

<sup>a</sup> Single Sr isotope analyses for non-leached whole-rock xenoliths.

<sup>b</sup> Mineral abbreviations: cpx, clinopyroxene; amph, amphibole.

<sup>c</sup> Sr and Nd isotopic compositions of cpx and amph in sample 4A-90-1 are from [Ionov et al. \(2002b\)](#).